Available online at www.sciencedirect.com

ScienceDirect

Geochimica et Cosmochimica Acta 296 (2021) 170–188

Geochimica et Cosmochimica Acta

www.elsevier.com/locate/gca

Volcaniclastic sandstones record the influence of subducted Pacific MORB on magmatism at the early Izu-Bonin arc

Anders McCarthy [a,*,1,2], Gene M. Yogodzinski [b], Michael Bizimis [b], Ivan P. Savov [c], Rosemary Hickey-Vargas [d], Richard Arculus [e], Osamu Ishizuka [f,g]

[a] Institute of Marine and Antarctic Studies, University of Tasmania, Castray Esplanade, Battery Point TAS 7004, Australia
[b] School of Earth, Ocean, and Environment, University of South Carolina, Columbia, SC 29208-3402 USA
[c] School of Earth and Environment, Institute of Geophysics and Tectonics, University of Leeds, Leeds LS2 9JT, United Kingdom
[d] Department of Earth and Environment, AHC5-394, Florida International University, Miami, FL 33199, USA
[e] Research School of Earth Sciences, Canberra, ACT 2601, Australia
[f] Geological Survey of Japan/AIST, Central 7, 1-1-1 Higashi, Tsukuba, Ibaraki 305-8567, Japan
[g] Research and Development Center for Ocean Drilling Science, Japan Agency for Marine-Earth Science and Technology, 2-15 Natsushima-cho, Yokosuka 237-0061, Japan

Received 13 September 2020; accepted in revised form 6 January 2021; Available online 16 January 2021

Abstract

The remnant rear-arc segment of the early Izu-Bonin arc, known as the Kyushu-Palau Ridge (KPR), is a key location where magmatic outputs can be constrained during the lifetime of an island arc. We present new geochemical data for coarse-grained basaltic to andesitic volcaniclastic sandstones derived from the KPR and deposited in the Amami Sankaku Basin (IODP Site U1438, Unit III rocks) in the time period 40–30 Ma. Bulk disaggregated and cleaned volcaniclastic sandstones of Unit III at Site U1438 retain primary magmatic signatures and can be used to infer the evolution of magmatic sources of the juvenile Izu-Bonin island arc through time. A sharp increase of slab-derived components to the source of KPR magmatism developed at about 35 Ma, indicated by increasing Th/La and decreasing Sm/La, Yb/Hf and Nb/Nd. Systematic variations in trace element ratios and increasing trace element abundances in younger samples through the 40–30 Ma time window are decoupled from Hf-Nd isotope ratios, which are measurably more depleted ($\varepsilon_{Hf} = 16.5–15$, $\varepsilon_{Nd} = 9.6–8.2$) than boninites produced during the preceding magmatic phase and sampled in the modern Izu-Bonin forearc. Hafnium isotopic compositions in the Unit III sandstones remain little-changed and similar to the subducting Pacific Plate after 40 Ma and do not revert to highly radiogenic compositions of the Indian-type MORB mantle wedge which is reflected in highly-depleted basalts produced at Site U1438 and in the forearc (commonly $\varepsilon_{Hf} \geq 18.0$). The overall pattern recorded in Unit III sandstones indicates that the Pacific-type MORB slab-melt component, which was present in the preceding boninite phase of magmatism, persisted after 40 Ma, while the subducted sediment component in the boninite source was lost or significantly reduced. Variations in trace element ratios (at constant ε_{Nd} and near-constant and radiogenic ε_{Hf}) and in high field strength element abundances of the early Izu Bonin arc are controlled by the addition of a subducted Pacific MORB melt or supercritical fluid to the mantle wedge. A subducted MORB (slab melt) component is thus sampled throughout the early life of the Izu-Bonin arc and in the currently active Izu-Bonin arc-backarc system.

* Corresponding author.
E-mail address: anders.mccarthy@utas.edu.au (A. McCarthy).
[1] Previously at School of Earth Sciences, University of Bristol, Wills Memorial Building BS8 1RJ, United Kingdom.
[2] Previously at Institute of Earth Sciences, University of Lausanne, 1015 Lausanne, Switzerland.

https://doi.org/10.1016/j.gca.2021.01.006
0016-7037/

Keywords: IODP Exp. 351; Izu-Bonin arc; Slab melt; Radiogenic isotopes, Kyushu-Palau Ridge

1. INTRODUCTION

Convergent plate boundaries produce arc magmas with distinctive chemical and petrological signatures compared to plume and ocean-ridge magmatism. Key trace element characteristics include enrichment in light rare earth elements (REE), and large ion lithophile elements (LILE; e.g., K, U, Cs, Rb, Ba), and depletion in high field strength elements (HFSE; Ta, Nb, Zr, Hf) as shown by Taylor and White (1965), Gill (1981), Pearce (1982) and others. In island-arc systems, these characteristics are attributed to source compositions and related processes that involve mixing of fluids and melts derived from subducted sediment and oceanic crust into the overlying mantle wedge. Distinguishing source contributions from the mantle wedge, subducting sediment, and oceanic crust is crucial to a complete understanding of arc magma formation, which is also thought to play a major role in the formation of continental lithosphere (e.g. Taylor and White, 1965; Shirey and Hanson, 1984; Kelemen, 1995).

A key location for identifying spatial-temporal changes in sources and processes contributing to the formation of arc magmas is in the Izu-Bonin arc, where initiation of subduction in an oceanic setting was succeeded by the production of a variety of primitive magma types during the initial growth and evolution of the nascent arc (e.g. Natland and Tarney, 1981; Bloomer and Hawkins, 1987; Stern and Bloomer, 1992; Cosca et al., 1998; Ishizuka et al., 2006, 2011a; Reagan et al., 2010; Li et al., 2019; Shervais et al., 2019; Ishizuka et al., 2020). In most arc systems, the earliest products of volcanism are buried beneath younger volcanic rocks and volcaniclastic sediment that accumulated during subsequent phases of arc growth. The implication of this common geologic succession is that the early history and evolution of arcs is recorded not only in the initial lavas and related intrusive rocks, but also in volcaniclastic sedimentary sequences deposited in basins proximal to the site of nascent arc growth (e.g. Egeberg et al., 1992; Bryant et al., 2003; Straub, 2003; Gill et al., 1994; Robertson et al., 2018).

Here, we target volcaniclastic sandstones and related conglomerate-breccias in drill core from International Ocean Discovery Program (IODP) Site U1438 in the Amami-Sankaku Basin (ASB) just west of the Kyushu-Palau Ridge (KPR), the site of Izu-Bonin subduction initiation (Fig. 1). A key advantage of the KPR and Site U1438 area is the chemical-temporal framework established by prior work (Arculus et al., 2015a,b; Yogodzinski et al., 2018; Brandl et al., 2017; Hickey-Vargas et al., 2018; Ishizuka et al., 2018; Hamada et al., 2020), which links initiation of Izu-Bonin subduction to eruption of an ultra-depleted form of MORB that is chemically much like FAB (forearc basalt of Reagan et al., 2010; Shervais et al., 2019), and subsequent changes in the mantle source regions of magmas forming the arc-backarc system. Biostratigraphic and radio-isotopic age constraints indicate most of the volcaniclastic rocks overlying the ultra-depleted basalt basement at Site U1438 were produced in the 30 – 40 Ma time window (Fig. 1) (Arculus et al., 2015a; Barth et al., 2017; Brandl et al., 2017; Waldman et al., 2020). This means the volcaniclastic record at Site U1438 captures activity that followed the depleted tholeiitic basalt – boninite to high-magnesian andesitic phase of volcanism between ca. 52–44 Ma (nascent arc) (Pearce et al., 1999; Ishizuka et al., 2011a, 2018, 2020) but preceded final construction and emergence of the KPR which is capped by volcanic rocks that are mostly 20–30 million years old (Ishizuka et al., 2011b).

The available record of the Izu-Bonin magmatism during this 10 Ma time period is sparse, recorded primarily by a limited number of fresh tephra layers recovered from the present-day frontal part of the arc (e.g. Bryant et al., 2003; Straub et al., 2010). Thus, the volcaniclastic sandstones from the Site U1438 drill core offer a key window into the early magmatic history of an intraoceanic arc system. We present chemical data from coarse-grained portions of volcaniclastic sandstones deposited from 40 to 30 Ma to constrain the temporal evolution of the juvenile Izu-Bonin arc following subduction initiation. We show that in this time-window, volcanism became progressively enriched in light REE and other trace element indicators of increasing contribution for a subducting plate. We discuss how this temporal growth in the arc trace element signature was produced in a manner that created no parallel changes in Nd isotope ratios and only a small shift in Hf isotope ratios to less radiogenic compositions. The stability of the isotopic record (indicated by the data presented here) implies a constancy of mantle wedge plus subducted Pacific MORB contributions through the 40–30 Ma time window of KPR growth, with only minor effects from subducting sediment. Finally, although volcanic glasses of tephra fallout from drill cores have been used extensively to constrain the evolution of the Izu-Bonin-Mariana arc (e.g. Egeberg et al., 1992; Arculus and Bloomfield, 1992; Bryant et al., 2003; Straub, 2003; Straub et al., 2010, 2015), we show that volcaniclastic sandstones deposited in arc-proximal basins represent a largely untapped record (e.g. Gill et al., 1994) that captures the evolution in time of source components contributing to the evolution of arc systems.

2. GEOLOGICAL SETTING OF UNIT III AND SAMPLES

Drilling at IODP Site U1438 (Arculus et al., 2015a,b) just west of the KPR (Fig. 1) penetrated oceanic crust formed of depleted tholeiitic basalts produced from ~ 49 to 47 Ma (Ishizuka et al., 2018). These lavas post-date the earliest magmatic rocks formed at the time of subduction initiation (Fig. 1). These rocks are low-K-Ti tholeiitic basalts and gabbros lacking traditional chemical indicators of subduction, and are derived from mantle sources more depleted by prior melt extraction than those involved in

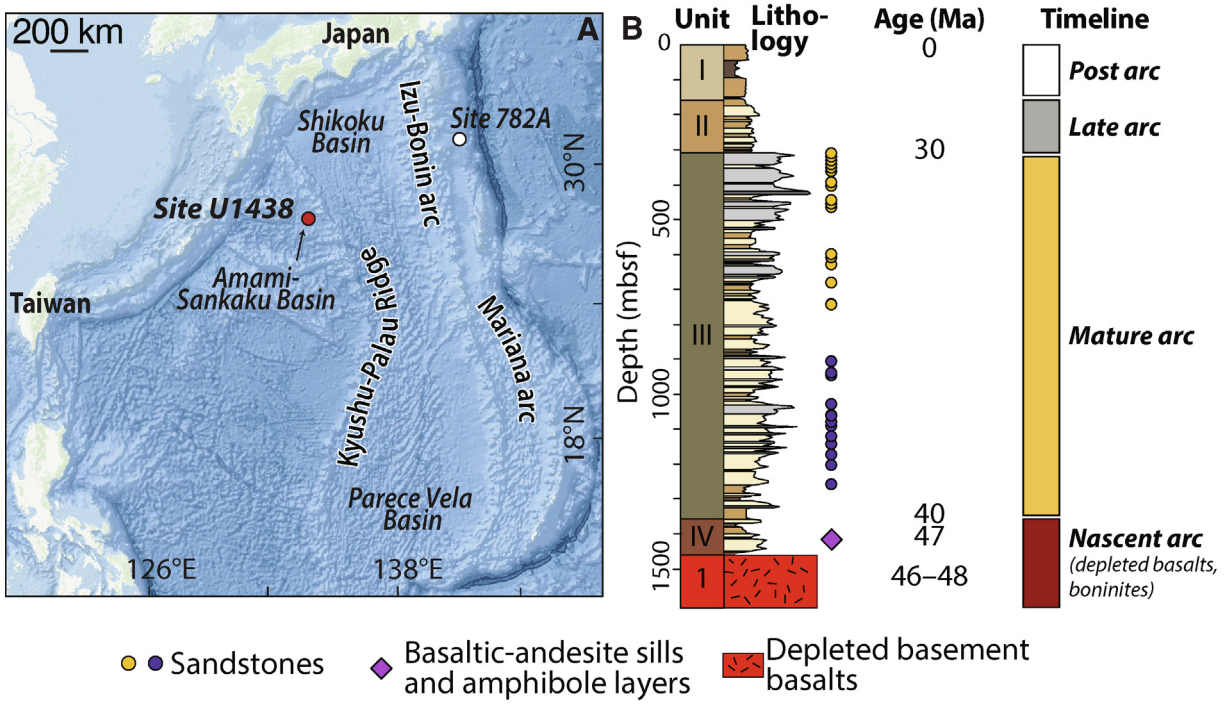

Fig. 1. (A) Location of the Amami-Sankaku Basin (IODP Site U1438) adjacent to the Kyushu-Palau Ridge; (B) Lithostratigraphy of Site U1438 (Arculus et al., 2015a) with location of sandstones (younger or older than 36 Ma, in yellow and purple colors respectively). The lithology column represents the average grain size of sediments (averaged over 5 m intervals), ranging from clay fraction (dark brown), silt (brown), very fine to fin sand (light brown), medium sand to coarse sand (grey) and gravel (dark grey) (after Arculus et al., 2015a). Ages after Arculus et al. (2015a), Brandl et al. (2017), Ishizuka et al. (2018) and Waldman et al. (2020). In B, Site U1438 timeline is based on Arculus et al. (2015a,b), Brandl et al. (2017), Yogodzinski et al. (2018), Hickey-Vargas et al. (2018), Ishizuka et al. (2018), McCarthy et al. (2019) and Waldman et al. (2020). Ocean Drilling Program (ODP) Site 782A lies along the Izu forearc basin (Shipboard Scientific Party, 1990).

the vast majority of MORB generation (Hickey-Vargas et al., 2018; Yogodzinski et al., 2018; Shervais et al., 2019; Li et al., 2019; Arculus et al., 2019; Reagan et al., 2019). This rock type has been termed forearc basalt (FAB) where it has been recovered from that present-day location (Reagan et al., 2010). It was generated in a near-trench setting and a narrow time window from 52 to 50 Ma (Reagan et al., 2019). This view has leads to a separate interpretation of chemically similar basement rocks at Site U1438 as products of backarc spreading after 50 Ma (Reagan et al., 2019). Alternatively, FAB and compositionally similar ultra-depleted basalts at Site U1438 and other locations immediately west of the KPR may have been produced by a common seafloor-spreading event spanning a broad swath of the arc throughout the 52–44 Ma time period of the growth of the nascent arc (Arculus et al., 2015b; Hickey-Vargas et al., 2018; Yogodzinski et al., 2018).

In the forearc, depleted basement is succeeded by boninite and high-Mg andesite dated at 51–44 Ma. This magmatic phase was succeeded in turn by arc basalt and andesite volcanism from 44 to 37 Ma which was the final episode of Izu-Bonin magmatism preserved in the present-day forearc (Lallemand, 2016; Reagan et al., 2019; Ishizuka et al., 2020). The sedimentary record that succeeded basement volcanism in the forearc is sparse, comprising mostly tuffaceous deep-sea sediment deposited after 34 Ma (Robertson et al., 2018). In contrast, the rear-arc record recovered at Site U1438 is nearly continuous: boninites are absent and depleted basaltic basement is succeeded by mudstone-dominated sedimentary sequences of Unit IV (Fig. 1), which are intruded by small-volumes of basaltic-andesite (Arculus et al. 2015a, Fig. 1). Some mudstones of Unit IV carry fresh, apparently volcanigenic, detrital biotite, amphibole, and zircon dated at ca. 47 Ma by $^{40}Ar/^{39}Ar$ and $^{238}U/^{206}Pb$ (Waldman et al., 2020). These products of early Izu-Bonin volcanism have relatively unradiogenic Hf ($\varepsilon_{Hf} < 14$) similar to the least radiogenic boninites (e.g. Li et al., 2019; Ishizuka et al., 2020) but distinct from Eocene to Oligocene Izu-Bonin tephra (Straub et al., 2010) and from volcanic units on forearc islands dated at 44 to 37 Ma (Ishizuka et al., 2020). Basaltic andesites that intrude Unit IV mudstones carry similarly unradiogenic Hf (Waldman et al., 2020). Thus, the record from Unit IV indicates that hydrous, basaltic-andesitic volcanism in the rear-arc at ca 47 Ma shared distinctive Hf isotope source characteristics with boninites that were produced contemporaneously in the forearc.

The 1000 meter-thick Unit III, which is the focus of this study, overlies the transitional Unit IV at Site U1438 (Arculus et al., 2015a; Johnson et al., 2017 (Fig. 1). Unit III is composed of fine-grained to coarse-grained volcaniclastic sandstones and conglomerates (data repository DR1 to DR2). This sedimentary unit is formed of a succession of distal gravity flows from volcanic eruptions or flank collapses originating from the growing volcanic edifices of the nascent Kyushu-Palau Ridge about 50 km east of Site

U1438 (Johnson et al., 2017; Brandl et al., 2017). Sandstones sampled for this study are from the depth interval 1300 and 300 meters below the sea floor (Fig. 1 and DR1). Biostratigraphic and radioisotopic age constraints (Arculus et al., 2015a; Barth et al., 2017; Ishizuka et al., 2018) indicate the samples were deposited successively between 40 and 30 million years ago (Fig. 1), with sedimentation rates estimated to vary between 30–180 cm/Ma over time (Brandl et al., 2017). Brandl et al. (2017) provide three distinct age models based on the uncertainty of the biostratigraphy, variation of grain size as a function of depositional rates, and sedimentary facie analysis, with the calculated depositional age of the sandstones based on their preferred age model. Volcanic clasts found in coarse intervals range between 0.5–3.0 cm in size. Volcanic minerals, especially pyroxene, plagioclase, and Fe-Ti oxides, are well preserved throughout Unit III (Arculus et al., 2015a; Brandl et al., 2017) (DR1 to DR2). Individual glass (formerly melt) inclusions (MI) hosted by clinopyroxene and plagioclase grains in Unit III range from basalt to rhyolite in composition (Brandl et al., 2017; Hamada et al., 2020). The mafic-silicic magmatism of Unit III occurring between ca. 40–30 Ma, thus records the compositional evolution of a developing chain of volcanic edifices defining a juvenile Izu-Bonin arc. The coincidence of biostratigraphic, paleomagnetic (Arculus et al., 2015a) and U-Pb zircon ages (Barth et al., 2017) from volcaniclastic rocks of Unit III indicate that material generated by volcanism at the KPR was erupted and then quickly transported and deposited in adjacent basins west of the KPR. The rapid deposition and limited transport minimized chemical alteration and mixing of different components prior to deposition, implying that the compositional evolution of these volcaniclastic sediments at Site U1438, some 50 km west of the KPR, records the evolution of the nascent juvenile Izu-Bonin arc over time (e.g. Brandl et al., 2017).

3. METHODS

Sample preparation steps described below were designed to isolate coarse volcaniclastic fractions from breccia-conglomerates and sand-sized grains in places where such coarse material exists in the core (DR1, DR2). Quarter-round samples from 5 to 8 cm in length each weighing 45 to 100 g were fragmented using the SelFrag^{TM} electro disintegrator at the University of Bern (UNIBE, Switzerland) to dislodge and disaggregate coarse fragments without crushing them. SelFrag operating conditions were 20 Pulses at 3 Hz, 140 kV, a 5 mm sieve inlay, and a 64 μm mesh to remove the finest grain sizes. Coarse-grained fractions from the SelFrag were dried and processed at the University of Bristol (UK). Samples were dry-sieved using the coarsest fraction (≥500 μm) for bulk chemical analysis (≥250 microns for sample U1438D 56R 7 W 36–42 due to the finer-grained nature of this sample). Samples were then sonicated in a solution of hexametaphosphate (5–10 gr/liter of H_2O) to dislodge and remove any remaining clay. This step was repeated 4–7 times until the solution was clear (DR2). Samples were then rinsed three times in MQ water and dried prior to being powdered in an agate ball mill container for 3–15 minutes. Loss on ignition (LOI) was determined by heating 2 g of sample to 1050 °C for 2 hours. A quantity of 1.2 g of the resulting powder was then mixed with 6 g of lithium tetraborate flux and fused at 1300 °C for 3.5 min in platinum crucibles prior to being quenched to form glass beads. Major element compositions were measured by a wavelength dispersive X-ray fluorescence spectrometry at the Institute of Earth Sciences, University of Lausanne (UNIL, Switzerland) on a PANalytical AxiosmAX fitted with a 4.0 KW Rh X-ray tube. The standards BHVO2 and AGV1 were used for quality control (Govindaraju, 1994). The relative standard deviation (RSD) of replicate standards ($n = 8$) is $< 0.13\%$ for most oxides, with slightly higher TiO_2 (0.71%), MgO (0.3%) and K_2O (0.42%). Trace element abundances were acquired on the flat side of the glass beads by quadrupole spectrometer Agilent 7700 (LA-ICP-MS) interfaced to a GeoLas 200 M ArF excimer ablation system (Institute of Earth Sciences, University of Lausanne). The laser was run at repetition rate of 10 Hz and an energy of 160 mJ, which is equivalent to 12 J cm^{-2}. Spot diameter was 75 to 100 μm. Sensitivity was maximized using the NIST SRM 612 glass standard (La^{139+}= 3.5x10^6 c.p.s., Th^{232+}= 5–5.5x10^6 c.p.s.). During this optimization, doubly charged ions (Ba^{2+}/Ba^{+}<2.7%) and oxide production rates (ThO^{+}/Th^{+}<0.08%) were minimized. Three repeat measurements were run on each bead. Helium was used as a cell gas carrier. Absolute trace element concentrations were determined using CaO previously measured by XRF as an internal standard and NIST SRM 612 as an external standard (Jochum et al., 2011). Data were processed using LAMTRACE software (Jackson, 2008).

Isotope ratios for Nd and Hf were measured in the Center for Elemental Mass Spectrometry (CEMS) at the University of South Carolina (USA). Approximately 200 mg of previously powdered fractions were weighed into Teflon capsules and leached for 30–45 min in closed capsules with 2.5 N HCl at 100 °C. Samples were then rinsed twice in 18MΩ H_2O and digested for 24 h in a 3:1 HF: HNO_3 mixture. Samples were sonicated after 12 h of digestion to help the process along. Following 24 h of digestion, the digested samples were then uncapped and heated on a hot plate to incipient dryness. Approximately 5 ml of 6 N HCl was then added. The capsules were sealed and heated to 100 °C for 1 hour, then uncapped and heated again to dryness. This step was repeated three times to remove fluoride precipitates. After the final digestion steps, the samples were rinsed into centrifuge tubes with 15 mL of 3 N HCl and centrifuged for 5 min at 5,000 rpm. Separate aliquots were pipetted for Nd and Hf column chemistry. Hafnium was separated using the method of Münker et al. (2001). Neodymium was isolated using standard cation exchange procedures. The bulk sample was processed though TRU-spec resin (Eichrom) in HNO_3 to separate a rare-earth element cut. Neodymium was then separated from this cut using LN-spec resin in HCl (e.g., Pin and Zalduegui, 1997).

Hafnium and Nd isotope ratios were measured using a ThermoFinnigan Neptune MC-ICP-MS in the CEMS at the University of South Carolina. Solutions were intro-

duced with a 100 ml self- aspirating Teflon nebulizer (ESI, USA) coupled to an ESI APEX-Q system. The samples were diluted to achieve a signal of 2–5 V on ^{143}Nd and ^{176}Hf, and 30–45 analytical cycles were run on each sample, depending on sample volume. Samples were bracketed every 3 solutions by the JNDi-1 standard for Nd, and the JMC-475 standard for Hf. Results were normalized to a ^{143}-Nd/^{144}Nd value of 0.512115 for the JNDI-1 standard, and a ^{176}Hf/^{177}Hf value of 0.282160 for JMC-475. Analysis of USGS rock standards run as unknowns (BHVO-2, AGV-2) agree with published reference values of Weis et al. (2006, 2007) to within 0.1–0.4 epsilon units. Epsilon values (ε_{Nd}, ε_{Hf}) were calculated with a CHUR value of 0.512630 for ^{143}Nd/^{144}Nd and 0.282785 for ^{176}Hf/^{177}Hf (Bouvier et al., 2008). Typical blanks for the CEMS labs are < 100 pg for Hf and < 20 pg Nd, and insignificant for the amount of analyte processed.

4. RESULTS

Major and trace elements and Hf-Nd isotopic compositions can be found in the electronic supplementary appendix. The sandstone samples are basaltic-andesitic to andesitic in bulk composition, with SiO_2 varying from 52.4 wt% to 60.5 wt% (anhydrous) and Mg#$_{Fetot}$, molar Mg/(Mg + Fe$_{tot}$)*100, from 63 to 44 (Fig. 2). They are low- to medium-FeO* and K_2O and are similar to volcanic rocks of the modern Izu-Bonin arc and to MI hosted in clinopyroxene and plagioclase separated from volcaniclastic rocks of Unit III (Brandl et al., 2017) (Fig. 2). Major oxide compositions and ranges of the sandstones are mostly uncorrelated with age; generally, there is no monotonic shift for example, from mafic to felsic with younging of the arc. Only TiO_2 (Fig. 2e) and P_2O_5 (Fig. 2f) show slight increases in the younger samples. Abundances of Na_2O show wide variation at constant SiO_2 and reach higher concentrations than in volcanic rocks of the modern Izu-Bonin arc (Fig. 2b). The extreme variability for Na_2O in the sandstones is likely a consequence of seawater alteration (*see discussion 5.1*).

Concentrations of incompatible trace elements in the sandstones, especially the light- to middle-rare earth element (REE), Th, Sr and high field strength element (HFSE), increase systematically in the younger samples (Figs. 3 and 4). Sandstones older than 36 Ma are flat in the middle and heavy REE and flat to slightly depleted in the light REE ($La_N/Sm_N = 0.9–1.8$) showing significant overlap with some depleted basement basalts (Fig. 5a). Sandstones of all ages

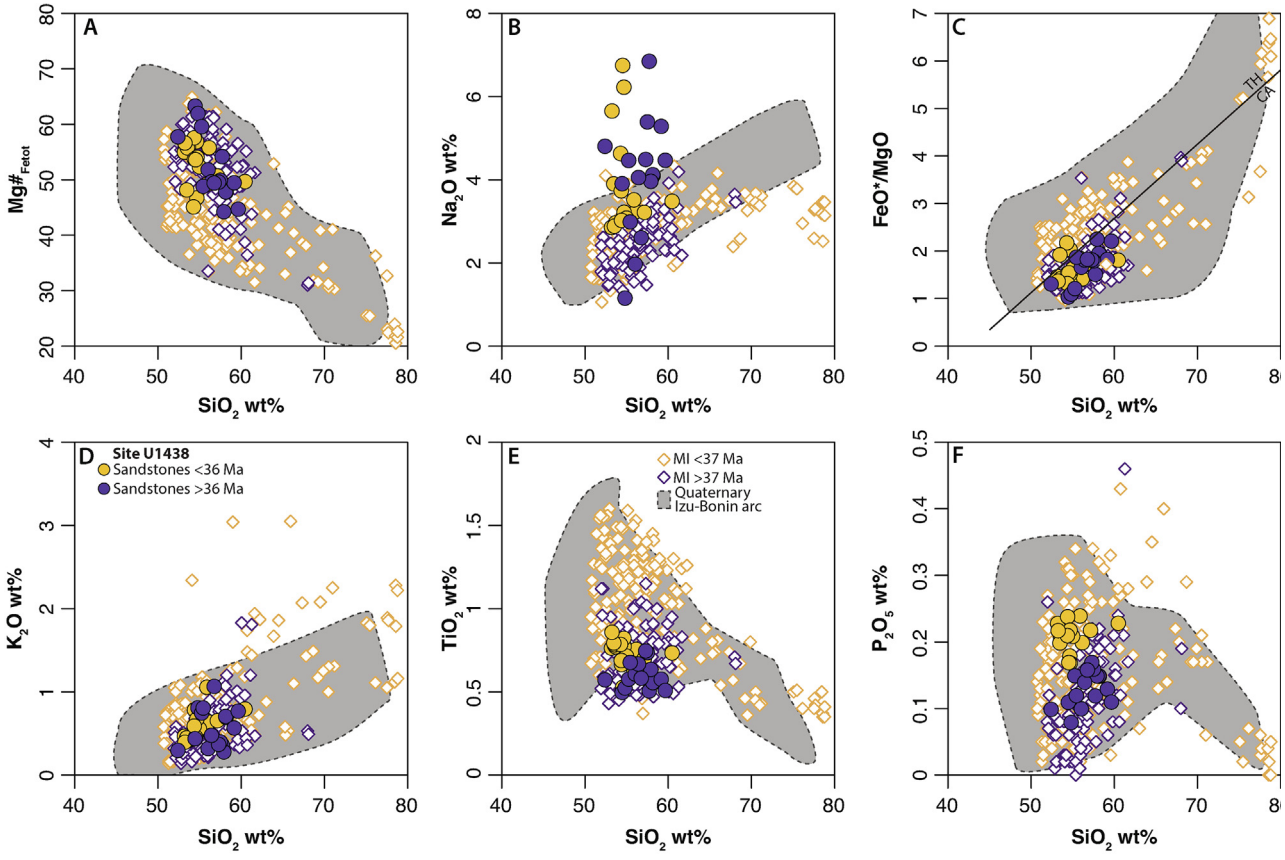

Fig. 2. (A–F) Major and minor oxide abundances of U1438 sandstone deposits showing Mg#$_{Fetot}$, Na_2O, FeO$_{tot}$/MgO, K_2O, TiO_2 and P_2O_5 vs SiO_2 wt%. Data for comparison include glass (formerly melt) inclusions (MI) from clinopyroxene and plagioclase from U1438 sandstones (Brandl et al., 2017). Note that in Brandl et al. (2017), the dataset is separated at ca. 37 Ma based on MI data. The grey field of the Quaternary Izu-Bonin rocks is from Straub (2017). Note that this field does not include high K_2O samples (2–4.5wt% K_2O), which are unlike typical Izu-Bonin arc rocks. The calc-alkaline (CA) – tholeiitic (TH) discriminant line in C is from Miyashiro (1974).

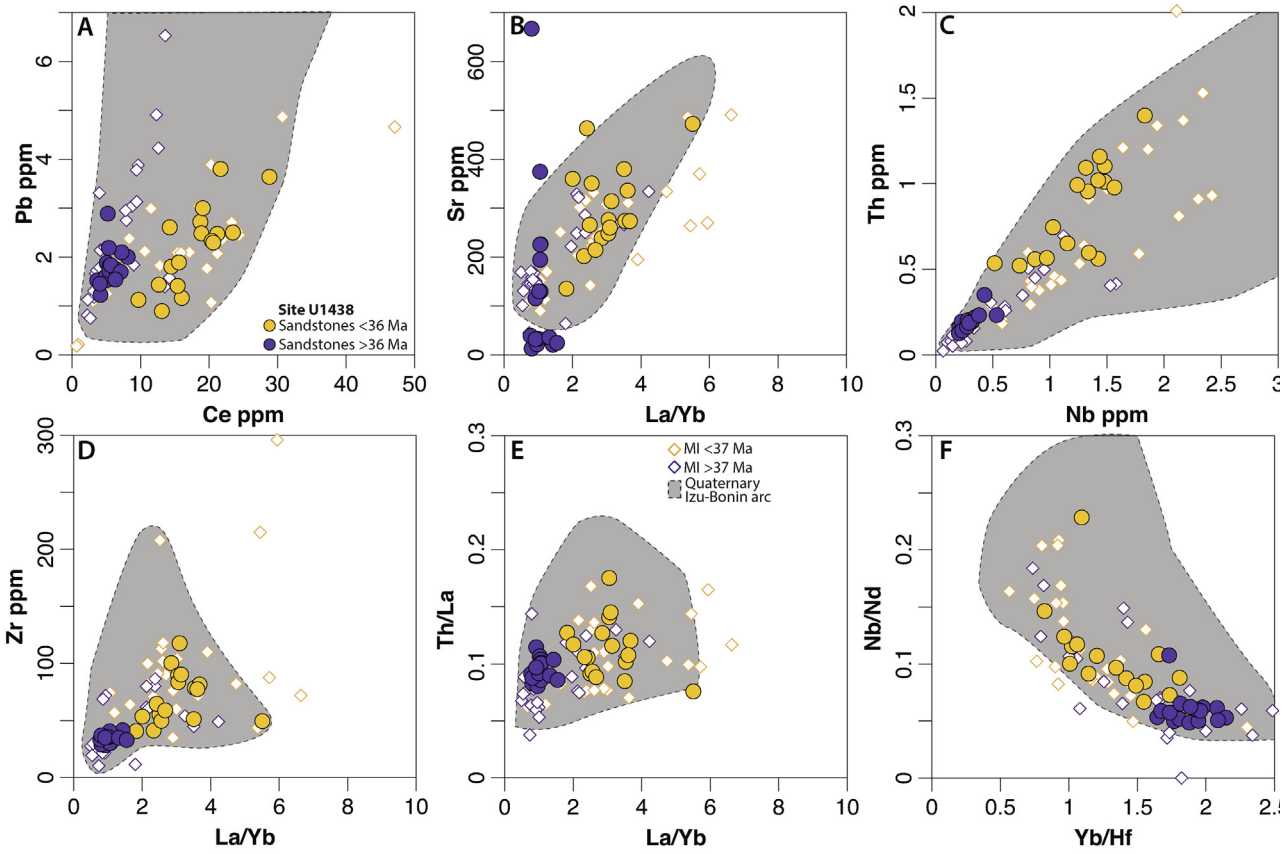

Fig. 3. (A–F) Bulk trace element abundances of U1438 sandstones and comparison to melt inclusions in silicates from the same Unit III sandstones (Brandl et al., 2017).

have similar heavy REE abundances (Fig. 5a) but samples younger than 36 Ma show a sharp enrichment in the light and middle REE ($La_N/Sm_N = 1.7–3.0$) compared to basement and to the older sandstones (Figs. 4 and 5, DR3). This gradual enrichment in the light and middle REE with time is well illustrated by normalizing the concentrations to the average ultra-depleted tholeiitic basalt (Unit 1) of the basement at site U1438 (Fig. 5b). Plotting the data in this way shows that there is roughly an order of magnitude enrichment in the light REE in the younger sandstones compared to the older group (Fig. 5b). A similar pattern is illustrated with multi-element plots normalized to primitive mantle (Fig. 5c,d). These show increased relative enrichments in the light and middle REE, Th, Zr, and Hf, combined with increased absolute Nb and Ta abundances and Nb/Ta with younging of the arc (Fig. 5).

Neodynium isotopic composition of sandstones are nearly constant through time, with MORB values of ε_{Ndi} from 8.2 to 9.6, and largely indistinguishable from depleted basement basalts and boninites (Fig. 6a). Hafnium isotope ratios in the sandstones are tightly clustered by age, with ε_{Hfi} greater than 16.0 in the older group and less than 16.0 in the younger group (Fig. 6b). Overall, the Hf-Nd isotopic compositions of sandstones fall within the middle of the total range of compositions defined by the older volcanic units seen in the boninites and depleted basement basalts (Fig. 5).

5. DISCUSSION

5.1. Alteration and primary characteristics of U1438 Unit III sandstones

The compositions of deep-sea sediments may be affected by seawater alteration, the addition of airborne continental material, and other sources of terrigenous sediment, tephra from volcanic eruptions outside of the Izu-Bonin system, and authigenic precipitates from seawater, such as Mn oxides and phosphates (e.g. Hein and Scholl, 1978; Vallier et al.,1980; Bienvenu et al.,1990; Gill et al., 1994; Patino et al., 2003; Robertson et al., 2018) (Fig. 7). To determine whether the bulk composition of sandstones can be used to infer magmatic processes along the KPR, we compare them to other external sources that might act as a contaminant, including the Japan arc, aeolian continent-derived sediment and Pacific marine sediments (Fig. 7). We use Rb/Hf, Zr/Y and Pb/Zr as proxies for contamination by such sediments (e.g. Robertson et al., 2018; Schindlbeck et al., 2018). These elements have been plotted versus major elements susceptible to hydrothermal alteration, sediment contamination and/or precipitation of iron-oxide crusts (e.g. K_2O, MnO, Na_2O). Fig. 7 shows that Rb/Hf (1.4–7.3), Zr/Y (2.0–5.3) and Pb/Zr (0.02–0.08, average of 0.04), MnO (<0.35 wt%), and K_2O (<1 wt%) in the Unit

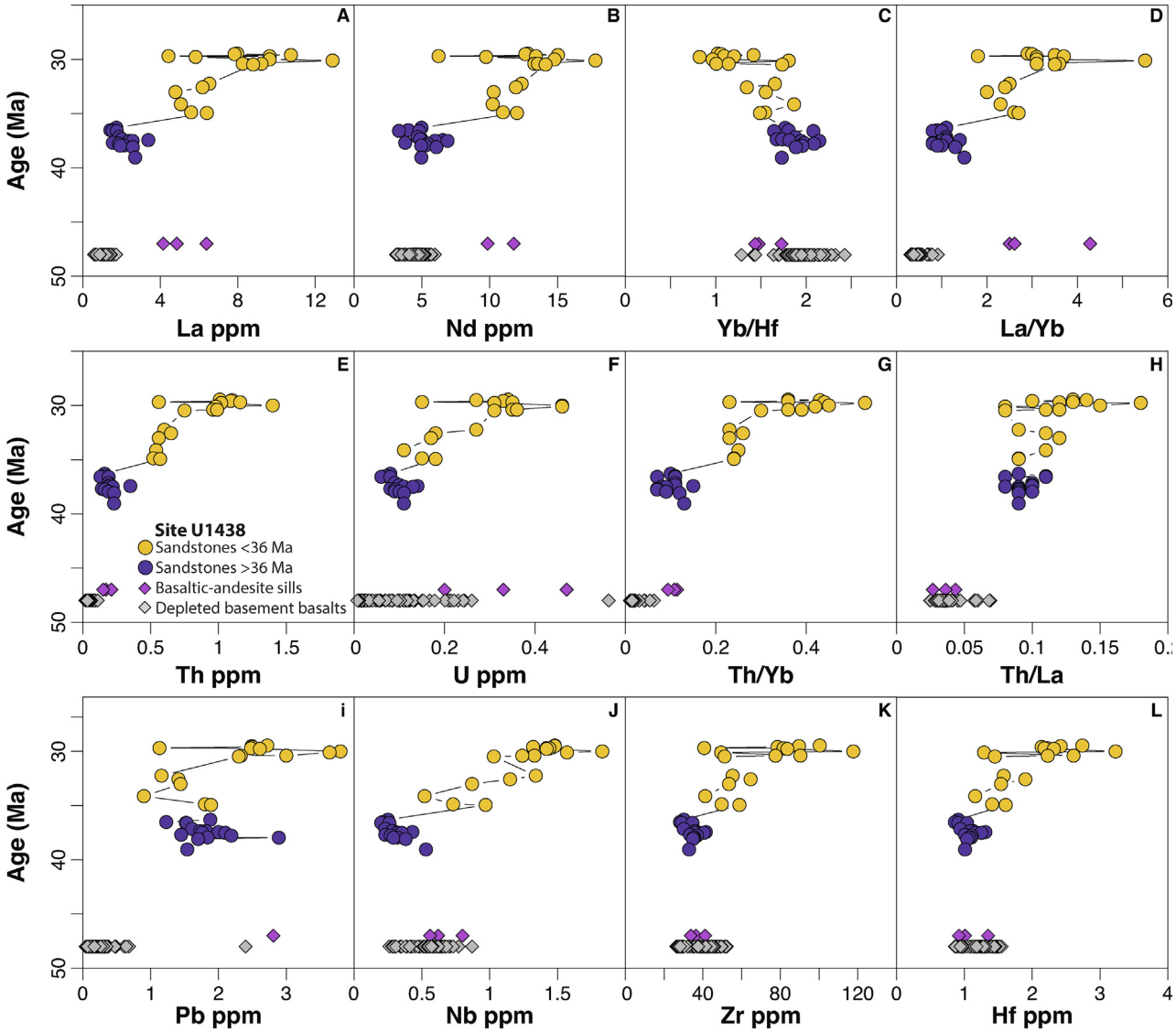

Fig. 4. (A–L) Secular changes in trace element abundances and trace element ratios of volcanic sandstones at Site U1438. The nascent arc represented by basaltic-andesite sills of Unit IV and depleted basement basalts of Unit 1 at Site U1438 are from Ishizuka et al. (2018) and Hickey-Vargas et al. (2018).

III sandstone are low and fall entirely within the field of Izu-Bonin arc lavas. If it were present in significant quantities, the continental detritus would produce higher Rb/Hf and Pb/Zr at higher K_2O wt% (Fig. 7a,c). The inclusion of oceanic sediments would lead to increasing MnO, or alternatively, higher Zr/Y (Fig. 7b). Thus, the dominant compositional signal in the Site U1438 sandstones appears to be KPR volcanism with minimal contamination from marine or continental sediment.

Unit III sandstones show increasing signs of alteration down-hole as shown by increasing clay and zeolite fractions in shipboard XRD analysis (Arculus et al., 2015a, DR1). Nonetheless, the bulk sandstone compositions show limited variability and fall entirely within the field of Izu-Bonin arc rocks. This includes elements easily affected by alteration (e.g. Pb, K_2O). The abundances of MnO, Ce, P_2O_5 remain low and within the field of the Izu-Bonin arc, implying a lack of precipitation of authigenic phosphates or Mn-Fe nodules (e.g. Robertson et al., 2018). Some alteration effects are evident in Sr and Na_2O, which show significant variation at near-constant SiO_2 or REE abundances (Figs. 2b and 3b). These elements are sensitive to seawater alteration and to the crystallization of zeolites at low temperature, consistent with the increasing down-hole presence of zeolites (Arculus et al., 2015a). This would also be consistent with processed separates from some samples which show a thin white coating on individual mineral grains and clasts prior to leaching, and which may reflect incipient crystallization of zeolite or carbonate (DR2). However, there is no systematic variation in Na_2O or Sr with REE or LOI (loss on ignition). As a result, Sr isotopic data have not been measured for the purpose of this study.

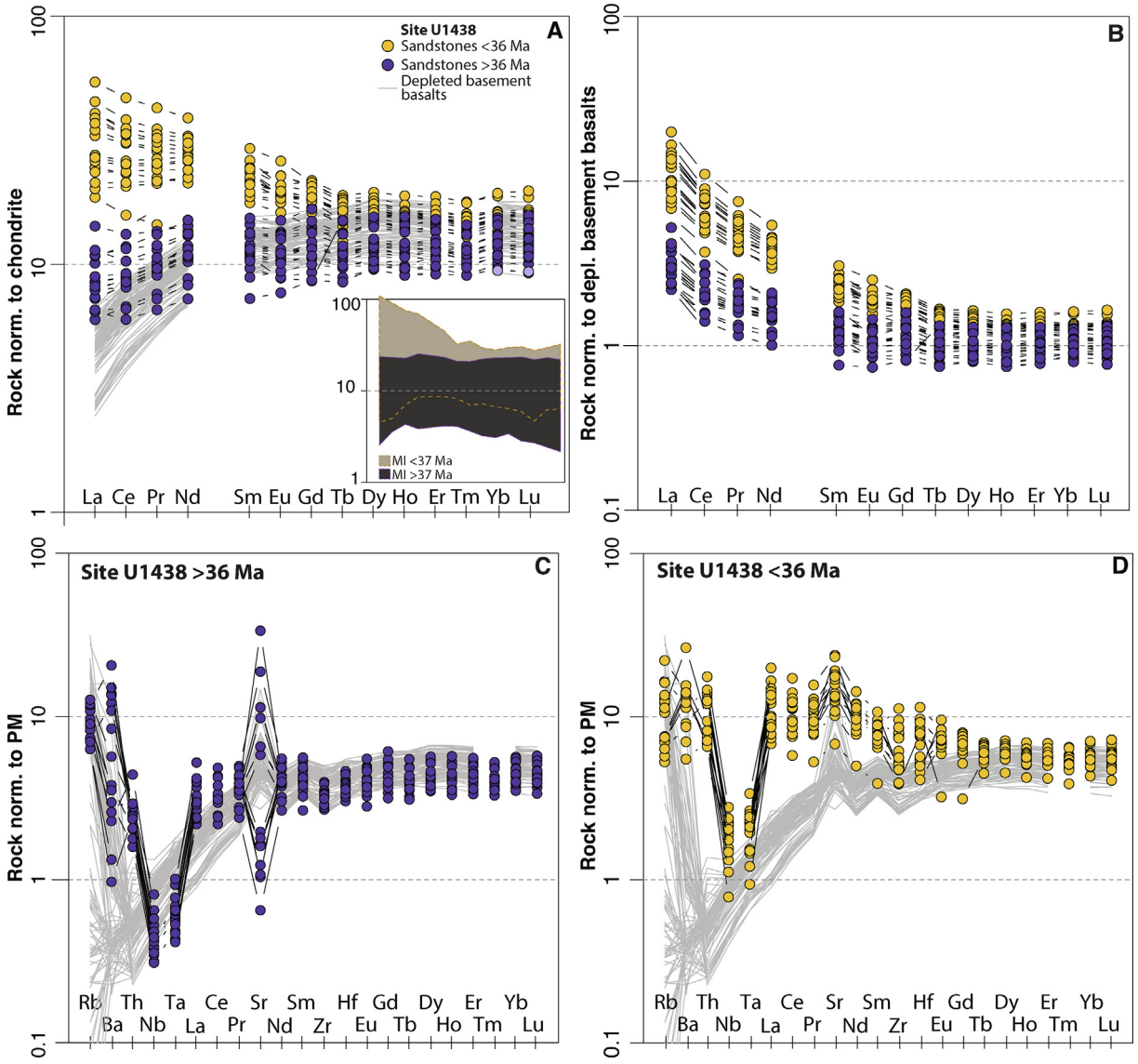

Fig. 5. (A and B) Bulk trace element abundances of U1438 sandstones. Chondrite and primitive mantle abundances from McDonough and Sun (1995). Depleted basement basalts from U1438 are from Hickey-Vargas et al. (2018). (C and D) U1438 sandstones normalized to Subunit E of Unit 1 depleted basalts of U1438 (Hickey-Vargas et al., 2018). Inset in (A) corresponds to REE field of melt inclusions (MI) from Brandl et al. (2017).

In Figs. 2, 3 and 5, we also compare our sandstones with glass inclusions from minerals separated from these same Unit III sandstones (Brandl et al., 2017). Both show similar trends of enrichment in minor and trace elements as samples get younger, including increasing TiO_2 and P_2O_5 (Fig. 2e,f), and increasing Sr, Th, REE and other HFSE (Fig. 3). These patterns are particularly well illustrated in Figs. 3b,d,e,f and 5a inset, where REE show enrichment trends similar to those in glass inclusions, albeit with more restricted compositional variability.

SelFraging of each bulk sandstone sample, followed by sieving and preservation of coarser fractions coupled with multiple rounds of deflocculating and leaching has removed most contamination (hydrothermal, biological or terrigenous/oceanic sediments) (DR1-DR2), which would otherwise affect the trace element abundances of these sandstones. This is consistent with cleaned separates generally showing a lack of clay fractions and showing unaltered clinopyroxene, plagioclase and distinct populations of unaltered volcanic lithic fragments (DR2). Thus, REE and HFSE variability through time in the Unit III sandstone cannot be a reflection of post-depositional alteration or contamination by pelagic/terrigenous components or precipitation of authigenic apatite and Mn-crust and must therefore reflect magmatic processes. We note further that Gill et al. (1994) previously found that with thorough cleaning of coarse sandstones deposited in proximal settings coupled to high sedimentation rates, as is the case for Site U1438 Unit III (e.g. Arculus et al., 2015a; Brandl et al., 2017; Johnson et al., 2017),

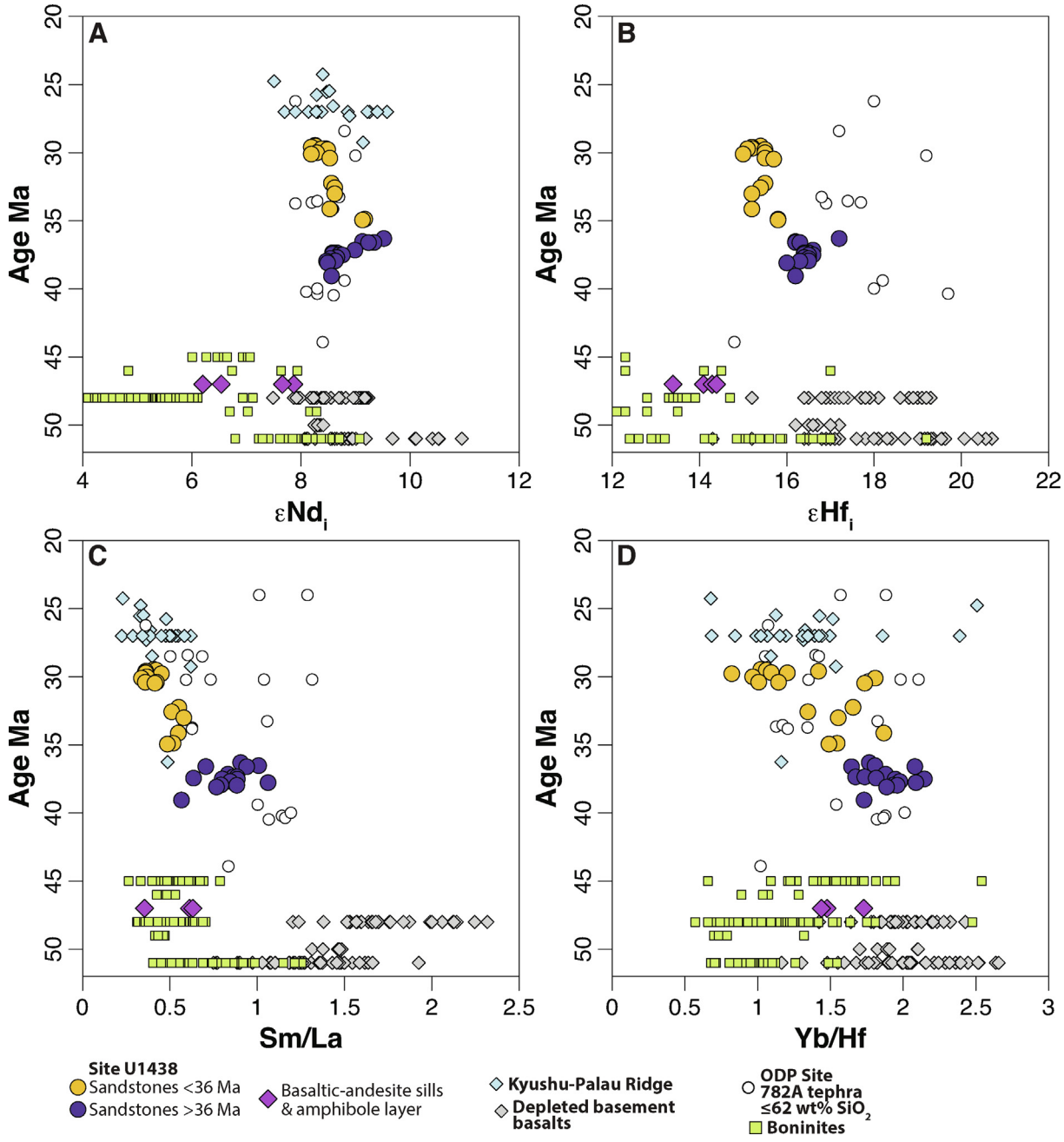

Fig. 6. (A–D) Depositional age (Ma) of sedimentary deposits vs ε_{Ndi}, ε_{Hfi}, Sm/La and Yb/Hf of sandstones . Depleted basement basalts from Yogodzinski et al. (2018), Hickey-Vargas et al. (2018), Reagan et al. (2010), Li et al. (2019). Kyushu-Palau-Ridge volcanism from Ishizuka et al. (2011b). ODP Site 782A tephra (restricted to tephra $\leq$ 62 wt% SiO_2) from Bryant et al. (2003) and Straub et al. (2010). Boninites are from Pearce et al. (1999), Reagan et al. (2010), Li et al. (2019) and Ishizuka et al. (2020). The age of amphibole layers and basaltic-andesite sills are from Waldman et al. (2020). Note that for the amphibole separate, isotopes are uncorrected for radiogenic ingrowth.

geochemical characteristics of magmatic arc sources may be elucidated.

5.2. Decoupling of trace element from isotope ratios

The basaltic and andesitic compositions of the Unit III sandstones are similar to Izu-Bonin volcanic rocks and remain generally constant through time (Figs. 2 and 3). In contrast, minor oxides and trace element abundances such as P_2O_5 (Fig. 2f), light REE, Th and HFSE (Zr, Nb, Ti) (Figs. 2e and 3–5) are higher in younger samples compared to older samples. The sandstones were deposited upon LILE- and HFSE-depleted basaltic oceanic basement formed at 49–47 Ma following subduction initiation

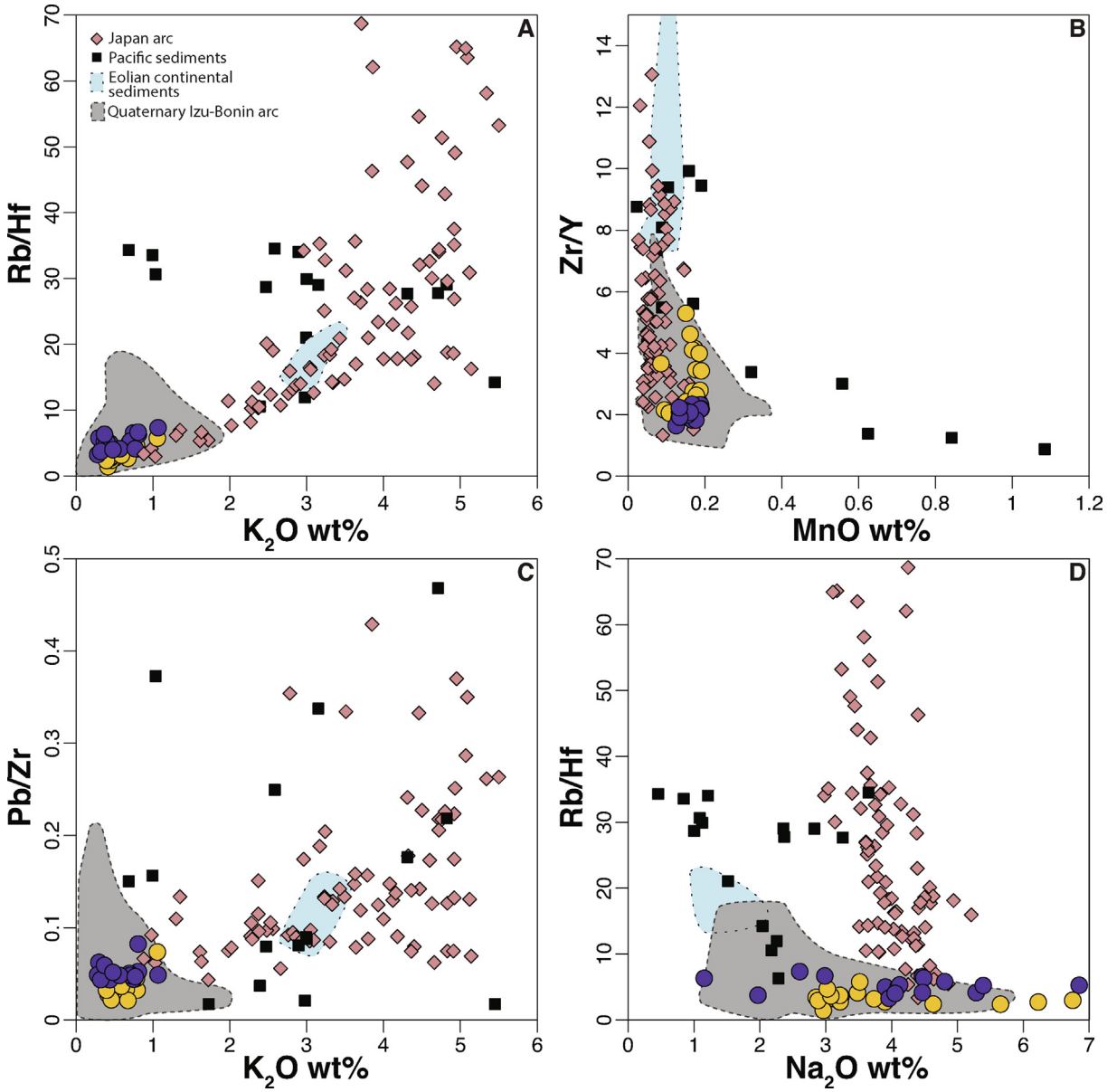

Fig. 7. Binary plots used to constrain sandstone alteration and contamination from different sources: (A) Rb/Hf vs K_2O wt%; (B) Zr/Y vs MnO wt%; (C) Pb/Zr vs K_2O wt%; (D) Rb/Hf vs Na_2O wt%. Pacific sediments are from ODP Site 801 (Vervoort et al., 2011) and ODP Site 1149 (Plank et al., 2007, Chauvel et al., 2009). Aeolian continent-derived sediments are from China (Liang et al., 2009). Japanese volcanism is from Kimura et al. (2015). Note that for (B), bulk MnO of sediments reach > 2 wt% (Vervoort et al., 2011).

(Ishizuka et al., 2018; Hickey-Vargas et al., 2018; Yogodzinski et al., 2018). As a result, observed secular changes in minor and trace elements (Fig. 4) are unlikely to be generated by assimilation and differentiation within the early arc crust. Therefore, increasing abundances of light REE and HFSE over time, which produce secular trends toward lower Sm/La, Hf/Nd and Yb/Hf (Figs. 3–8) must reflect changes in the source(s) of KPR volcanism following the end of the nascent phase of Izu-Bonin arc growth (Fig. 1).

Isotopic compositions of basaltic and andesitic volcanism recorded in KPR volcanic rocks and Site U1438 sandstones show only minor shifts of less than 1.5 epsilon units toward less radiogenic Hf and Nd over the span of 10 Ma (Fig. 6a,b). Limited variability in Hf and Nd isotopic compositions of the sandstones contrast with the more heterogeneous, depleted basalts and boninites that make up the nascent Izu-Bonin arc (Fig. 6a,b). The consistently radiogenic and MORB-like signature of the sandstones is surprising considering the increasing abundances of fluid-immobile HFSE and REE over time (Figs. 4, 6c,d and 8). The trend toward more enriched trace element patterns with roughly constant and MORB-like Hf and Nd isotopes is similar to the younger volcanic rocks along the northern segment of the KPR erupted between 20–30 Ma (Savov et al., 2006; Ishizuka et al., 2011b) (Fig. 6). The Unit III sandstones show consistent shifts toward lower Sm/La, Yb/Hf and slightly higher Th/La in younger samples

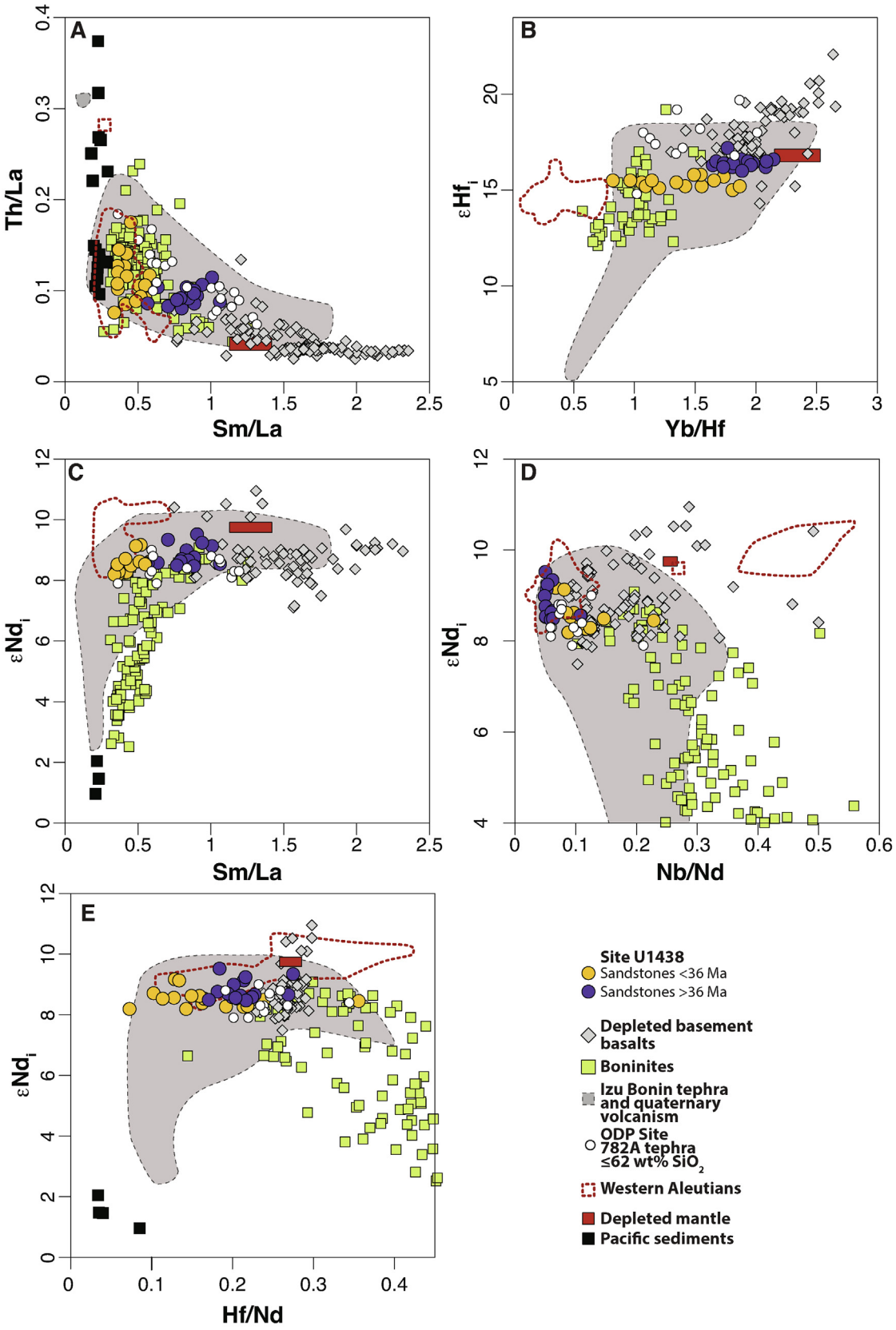

Fig. 8. Trace element ratios and isotopic compositions as a function of trace element ratios; (A) Th/La vs Sm/La; (B) εHf_i vs Yb/Hf; (C) εNd_i vs Sm/La; (D) εNd_i vs Nb/Nd; (E) εNd_i vs Hf/Nd. Western Aleutian lavas are from Yogodzinski et al. (2015). Depleted MORB Mantle is from Workman and Hart (2005). Field of Izu-Bonin arc includes Quaternary volcanic rocks from Straub (2017) and Tollstrup and Gill (2005) as well as Izu-Bonin tephra from Bryant et al. (2003) and Straub et al. (2010). Izu-Bonin arc rocks trending towards unradiogenic Hf and Nd isotopic ratios (Kasuga seamount) are dominated by a sediment-melt component (Tollstrup and Gill, 2005).

(Figs. 6 and 8a). Changes in fluid-immobile trace element ratios of this type are generally interpreted to reflect the addition of subducted sediment or melt derived from subducted sediments in the source (Pearce et al., 1995; Plank, 2005; Tollstrup and Gill, 2005; Chauvel et al., 2009; Tollstrup et al., 2010). However, secular changes in trace element ratios in Unit III sandstones toward lower Sm/La, Hf/Nd, and Yb/Hf are not linked to shifts toward less radiogenic Hf and Nd which would be required if the cause was subducted marine sediment (Figs. 6c,d and 8b–e). The limited influence of subducted sediment on the evolution of isotopic ratios at Site U1438 is well illustrated by mixing trends involving sediment end-members which always produce trajectories toward lower ε_{Nd} with only minor shift towards lower ε_{Hf} (Fig. 9a,b) as well as moderate shifts in HFSE/REE ratios with concomitant changes towards unradiogenic ε_{Nd} (nearly vertical mixing lines in Fig. 9c). These changes required by the involvement of sediment in the source are opposite to the Unit III volcaniclastic sandstone trends at Site U1438, which change in time toward unradiogenic Hf (by one to two epsilon units) at nearly constant εNd (Fig. 9a,b) and are likewise widely variable in Hf/Nd at nearly constant ε_{Nd} (Fig. 9c). Thus, no mixing line from a well-constrained Indian-MORB mantle to any Izu-Bonin sediment composition can produce the Hf-Nd isotope data patterns observed in the Unit III sandstones (Fig. 9).

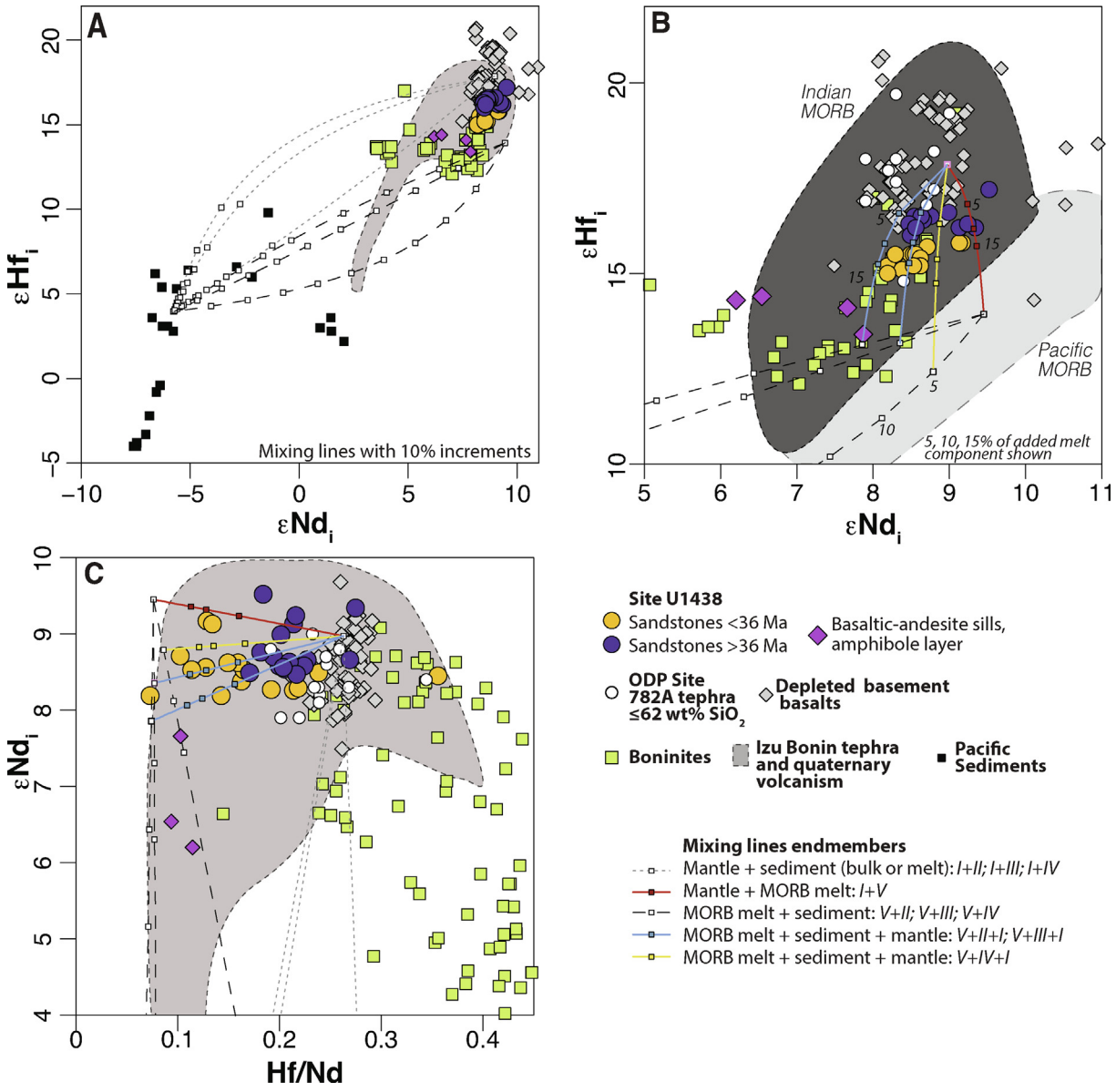

Fig. 9. (A and B) εNd_i versus εHf_i for Unit III samples compared with end-member mixing models with three end-member compositions: an Indian-type depleted mantle source (D-DMM), Pacific MORB slab melt and Pacific sediments. Red line corresponds to mixing between a D-DMM and a MORB melt, whilst yellow and blue lines correspond to a slab melt (MORB + sediments) added to a D-DMM. For mixing components I to V, see Table 1. (C) Hf/Nd versus εNd_i with the same mixing-trends as in (A and B).

Linked trace element and isotopic changes observed during the growth of the nascent arc, and specifically the transition from depleted tholeiitic basalts to boninites, provides additional constraints on the nature of secular changes in Unit III sandstones. A key change during the growth of the nascent arc is in the record for Hf isotopes, which become more unradiogenic by an average of ~ four epsilon units in the basaltic andesites of Unit IV and in boninites (average $\varepsilon_{Hf} \sim 14$) compared to the preceding episode of depleted basalt volcanism (average $\varepsilon_{Hf} \sim 18$) (Fig. 6b, Fig. 9b). This isotopic shift is interpreted to reflect a change in the dominant source of Hf from Indian-type MORB mantle to Pacific-type MORB of the subducting oceanic crust in the form of a slab melt (Li et al., 2019). Following the end of boninite volcanism at ~ 45 Ma there is, importantly, no reversal in Hf isotopic ratios back toward more radiogenic compositions ($\varepsilon_{Hf} \sim 18$) as would be expected if the source of Hf in the sandstones were Indian-type MORB in the mantle wedge, and if Hf isotope ratios in products of KPR volcanism were predominantly a reflection of the mantle source end-member (i.e., Pearce et al., 1999; Straub et al., 2010). This constraint is particularly strong because we know from the compositions of the depleted basalts that make up the basement throughout the Izu-Bonin system, that the mantle wedge below the KPR had the composition of Indian-type MORB, commonly with $\varepsilon_{Hf} \geq 18.0$ (Yogodzinski et al., 2018; Li et al., 2019) (Fig. 9b). The persistence of relatively unradiogenic Hf in the sandstones (similar to the most radiogenic boninites with $\varepsilon_{Hf} \sim 16.0$) compared to more radiogenic compositions expected from an Indian-type of MORB mantle and seen in the underlying basement basalts clearly indicate that the physical conditions of slab melting that are required to explain the Hf isotope ratios and other characteristics of the boninites (Pearce et al., 1992; Li et al., 2013, 2019) must have persisted throughout the 30–40 Ma time window when volcanism at the KPR produced the Unit III sandstones. It is also important to emphasize that boninites with least radiogenic Nd and Hf isotopic ratios also have relatively low Sm/La and Yb/Hf and high Th/La which are consistent with the presence of a sediment source component (Fig. 8a–c), but which are mostly absent from the Unit III sandstones. The dominant source of light REE, Hf, Nb, and (likely) other HFSE in the products of KPR volcanism that were eventually incorporated into the Site U1438 Unit III sandstones, were derived predominantly from the subducting oceanic crust with little or no contribution from subducted sediment or sediment melts.

5.3. Influence of subducted Pacific MORB on the evolution of Izu-Bonin Magmatism

A contribution of subducted Pacific MORB to the trace element and isotopic signature of KPR magmatism can be illustrated by mixing lines in ε_{Hf} versus ε_{Nd} (Fig. 9a,b) and ε_{Nd} versus Hf/Nd plots (Fig. 9c). Changes in fluid-immobile trace element abundances concomitant with the observed shifts in Hf-Nd isotopic ratios can be explained by the addition of MORB slab melt to a D-DMM, leading to shifts in Hf/Nd at near-constant ε_{Nd} as well as gradual shifts towards less radiogenic Hf isotopic ratios. A contribution of 2.5% to 15% of a slab melt (composed of 0–10% sediment melt and 90–100% Pacific-MORB melt) added to a depleted mantle wedge signature can explain the spectrum of U1438 sandstone compositions (Fig. 9).

It is notable that Nd and Hf isotopic compositions of the Unit III sandstones remain within the field of Indian MORB throughout the 40–30 Ma time period even though Pacific MORB melt is added to an Indian D-DMM (Fig. 9b). Under this interpretation, the source in this time period is primarily a mixture of two depleted components: an Indian-type mantle source and a subducting Pacific-type oceanic crust. However, it is impossible to rule out a sudden influx of heterogeneous and enriched Indian-MORB mantle to explain the isotopic data (e.g. Brandl et al., 2017). For example, shifts in Hf-Nd isotopic ratios of coeval tephra along the Izu-Bonin forearc (Fig. 9b) (ODP Site 782A, Straub et al., 2010) have been interpreted as the sampling of a heterogeneous mantle, with the majority of Hf and Nd budget from the Izu volcanic front therefore originating from the mantle (Straub et al., 2010). This interpretation is based on the lack of enrichment in trace elements concomitant with the lack of isotopic shift toward less radiogenic Hf-Nd isotopic ratios (Straub et al., 2010), which should be observed if sediment or MORB melt contributed to arc magmatism. This can also be seen in Fig. 6, where coeval tephra ($\leq$62 wt% SiO_2) from the frontal part of the arc typically have less enriched L-REE patterns and more radiogenic Hf isotopic ratios than Site U1438 volcaniclastic sandstones. Of particular note, these tephra show a clear overlap with the field of Hf–Nd isotopic ratios defined by spatially extensive eruption of depleted basement basalts, and by inference the underlying depleted Indian-MORB mantle, prior to the growth of the juvenile Izu-Bonin arc (e.g. Reagan et al., 2010; Yogodzinski et al., 2018; Li et al., 2019) (Fig. 9b). Such a depleted mantle source is still sampled in the modern Izu-Bonin arc (Yogodzinski et al., 2018). This isotopic overlap between depleted basement basalts and basaltic to andesitic tephra of Site 782A suggests that volcanism along the volcanic front could be sampling an inherently heterogeneous mantle with little to no contribution of Nd and Hf from a subducted sediment or MORB melt (Straub et al., 2010).

However, unlike 30–40 Ma tephra sampled in the modern forearc, an influx of a heterogeneous mantle along the rear-arc at Site U1438 cannot explain the secular growth of slab-derived components reflected in the trace element ratios and Hf-Nd isotopic compositions of Unit III sandstones ((Figs. 3–5). Such linked trace element and isotopic changes through time are more plausibly explained by the addition of subducted Pacific MORB slab melt to a depleted Indian MORB mantle source below the nascent Izu-Bonin arc (Fig. 9b,c). In fact, this source mixture was already present during the earlier boninite and Mg-andesite stage of protoarc magmatism that followed subduction initiation at 50–52 Ma and preceded deposition of the Unit III sandstones starting at ~40 Ma (e.g. Li et al., 2019; Ishizuka et al., 2020). In this time period, the isotopic shift was primarily one of declining εHf with relatively little change in εNd along a path connecting

Table 1
End-member compositions for modeling of mixing compositions. An Indian-MORB field can be constrained by the isotopic characteristics of depleted basement basalts formed upon (or following) subduction initiation. As these basalts form as a consequence of extensive partial melting of an Indian-type depleted DMM (Hickey-Vargas et al., 2018; Yogodzinski et al., 2018), our mantle end-member is therefore a D-DMM from Workman and Hart (2005) with isotopic compositions from a representative subset of Site U1438 depleted basalts (Yogodzinski et al., 2018) (I). For sediments, we use a bulk sediment composition of ODP Site 1149 (Plank et al., 2007; Chauvel et al., 2009) (II) as well as a calculated sediment melt (III) based on the bulk sediment composition of ODP Site 1149 corrected for an average sediment enrichment factor based on experimental data from Hermann and Rubatto (2009) and Skora and Blundy (2010) (see Yogodzinski et al. (2015) for further details). To illustrate the effect of variations in sediment composition on mixing-lines, an additional sediment melt endmember based on melting of Aleutian sediments at 900 °C and 4 Gpa from Yogodzinski et al. (2015) is also shown for comparison (IV). The Pacific-MORB endmember (V) is defined by the isotopic composition of an average of Pacific MORB (Chauvel and Blichert-Toft, 2001; Gale et al., 2013) with the calculated slab melt composition from Yogodzinski et al. (2015) based on experimental partition coefficients from Kessel et al. (2005) at conditions of 900 °C and 4 Gpa.

Endmember	Hf (ppm)	$^{176}Hf/^{177}Hf$	Nd (ppm)	$^{143}Nd/^{144}Nd$	References
I. Mantle wedge (D-DMM)	0.127	0.283290	0.483	0.513090	Workman and Hart (2005), Yogodzinski et al. (2018)
II. Bulk sediment, ODP Site 1149	1.44	0.282897	25.20	0.512336	Plank et al. (2007) Chauvel et al. (2009)
III. Sediment melt, ODP Site 1149	1.36	0.282897	16.73	0.512336	Chauvel et al. (2009)
IV. Sediment melt (Aleutian sediments)	2.93	0.282897	9.76	0.512336	Yogodzinski et al. (2015), Chauvel et al. (2009)
V. Pacific MORB slab melt	0.862	0.283179	11.30	0.513114	Yogodzinski et al. (2015), Gale et al. (2013)

depleted basalts with $\varepsilon_{Hf} \sim 17.5$ (Indian-type MORB) to the most radiogenic boninites with $\varepsilon_{Hf} \sim 12.5$ (Fig. 9a-b). Addition of sediment created a second trend in the boninites and andesite sills from Site U1438 which connects the most radiogenic boninites with $\varepsilon_{Nd} \sim 8.2$ to the least radiogenic boninites with $\varepsilon_{Nd} = 5–6$ and with relatively little change in ε_{Hf} (Fig. 9a and b) (Li et al., 2013, 2019; Ishizuka et al., 2020) (Fig. 9). The contribution of Pacific-MORB melt is also illustrated in broadly variable in Hf/Nd with constant Nd isotopic ratios for boninites with $\varepsilon_{Nd} > 8.0$ (Fig. 9c). Similar variability is illustrated by 47 Ma basaltic andesites and detrital amphiboles in Unit IV at Site U1438 (Fig. 9), with $\varepsilon_{Nd} < 8.0$ and requiring significant sediment in the source (Fig. 9c). Thus, the change that followed the boninite phase of protoarc volcanism, which is recorded in Unit III sandstones at Site U1438, indicates that the Pacific-type MORB component (likely produced by melting of subducting oceanic crust) persisted after 40 Ma, while the subducted sediment component was lost or significantly reduced (Fig. 9). This demonstrates that sediment contributions to the arc-magma source can wax and wane independently of the slab-melt component, possibly reflecting episodes of sedimentary accretion and subduction erosion in the forearc (e.g., von Huene and Scholl, 1991; Kay et al., 2005; DeCelles et al., 2009).

These changes throughout the 40–30 Ma time window are consistent with other geochemical patterns along and across the modern Izu-Bonin and Northeast Japan arcs. To the north, Hanyu et al. (2006) interpreted a shift of decreasing ε_{Hf} to imply the melting of subducted oceanic crust upon back-arc spreading along the Northeast Japan arc. Pineda-Velasco et al. (2018) also find in this setting, that high-Sr (adakitic) volcanism is linked to seismic gaps in the slab, indicating that melting of the slab is focused around tears or openings in the subducting plate (e.g. Yogodzinski et al., 2001). Izu-Bonin arc magmas also show significant shifts in trace element and isotopic characteristics across the arc, from the volcanic front to rear-arc (e.g. Hochstaedter et al., 2001; Pearce et al., 2005; Tollstrup and Gill, 2005; Tollstrup et al., 2010). Magmatism along the volcanic front shows effects of aqueous fluid enrichment (Hochstaedter et al., 2001; Straub et al., 2004; Pearce et al., 2005; Tollstrup et al., 2010) that may include a sediment-melt component (e.g. Tollstrup and Gill, 2005). In contrast, rear-arc magmatism shows a waning of the aqueous slab flux and a significant increase in fluid-immobile elements, enrichment in L-REE and a shift towards less radiogenic Hf as a consequence of a supercritical fluid or melt composed of > 90% of AOC and < 10% sediments (Tollstrup et al., 2010). Unit III sandstones from Site U1438 show shifts towards somewhat less radiogenic Hf isotopic ratios (Fig. 9b) coupled to enriched trace element patterns which are more typical of present day Izu-Bonin magmatism in the rear-arc (e.g. Tollstrup et al., 2010) than coeval tephras from the frontal part of the arc (ODP Site 782A, Bryant et al., 2003; Straub et al., 2010) (Figs. 6 and 9b). Our results are therefore similar to those of Tollstrup et al. (2010) and Freymuth et al. (2016) which indicate that the composition of arc magmas are con-

trolled in part by the initiation of partial melting of altered oceanic crust below the arc as well as a waning influence of subducted sediments towards the rear-arc.

Finally we note that a secular shift from Indian- toward Pacific-type MORB compositions is not unique to the Izu-Bonin arc. This shift is documented along the rear-arc and back-arc of the southern New Hebrides-Hunter Ridge (North Fiji Basin), where primitive high-Mg# arc magmas with slab-melt (adakitic) characteristics show Pacific-MORB signatures in a system where the composition of the mantle wedge is that of Indian-type MORB (Monzier et al., 1994; Heyworth et al., 2011; Patriat et al., 2019). This shift has been explained by a number of mechanisms including involvement of a heterogeneous mantle source in the form of a trapped Pacific-MORB mantle (Pearce et al., 2007), but widespread high-Mg# and adakitic magmatism leads us to favor the slab-melt interpretation (Patriat et al. 2019). In addition, the Western Aleutians represents a geodynamic setting where low subduction rates and highly oblique convergence leads to partial melting of the basaltic section of the subducting oceanic plate (Yogodzinski et al., 1995, 2017; Kelemen et al., 2003). Products of adakitic magmatism in the western Aleutians include an abundance of primitive, high-Mg# volcanic rocks that have strongly fractionated and arc-like trace element patterns that are linked to essentially constant and MORB-like Nd-Hf isotopic compositions and widely variable Hf/Nd with no more than a minor role for subducted sediment or altered oceanic crust (Yogodzinski et al., 1995, 2017) (Fig. 8). Site U1438 volcaniclastic sandstones record similar systematic shifts in REE/HFSE ratios at near-constant Hf-Nd isotopic ratios (Fig. 8b–e) similar to younger KPR magmatism at 30–20 Ma (Ishizuka et al., 2011b) (Fig. 6). These trends outlined by western Aleutian magmatism and Site U1438 sandstones are however distinct from a significant portion of Izu-Bonin arc lavas, tephra and boninites which show important shifts in REE/HFSE and concomitant shift towards unradiogenic Nd and Hf isotopic ratios (Figs. 8 and 9) related to sediment melts/fluids and AOC-type fluids (e.g. Tollstrup and Gill, 2005). Contrasting the Western Aleutian and New Hebrides-Hunter-Ridge systems, Izu-Bonin magmatism does not generally show major element evidence of slab melting, which is reflected primarily in primitive, high-Mg# andesites and dacites characterized by relatively low ratios of FeO* and CaO to Al_2O_3 (e.g. Yogodzinski et al., 1994, 1995; Li et al., 2013). This likely reflects a combination of processes: firstly, reactive melt percolation and crystallization within the mantle wedge leads to re-equilibration of major elements and a dampening but ultimately preservation of the distinctive pattern of trace element ratios associated with arc volcanism (e.g. Yogodzinski et al., 1995; Rapp et al., 1999); secondly, enhanced flux melting of the mantle wedge and dominance of basalt is characteristic of much Izu-Bonin arc magmatism (cf. Aleutians as modeled by Kay, 1978; Kelemen et al., 2003; Yogodzinski et al., 2015). Such shifts in composition are well illustrated along the Aleutian arc as the contribution of slab- versus mantle wedge melting to arc magmatism diminishes eastward along the Aleutian arc (Kelemen et al., 2003; Yogodzinski et al., 2015).

We conclude that Unit III sandstone data of the early Izu-Bonin arc, in conjunction with recent experimental datasets of dehydrating and melting of subducted MORB (Kessel et al., 2005; Louvel et al., 2013; Carter et al., 2015; Tsay et al., 2017) and with geochemical evidence derived from the western Aleutian arc (e.g. Yogodzinski et al., 2010, 2015), indicates that HFSE are mobilized from the basaltic section of a subducting slab as slab-melts or super-critical fluids at conditions relevant to arc magmatism and are therefore unlikely to act as conservative elements in subduction zones as generally assumed (Pearce et al., 1999, 2007; Straub et al., 2010, 2015).

6. CONCLUSIONS

Hafnium-Nd isotopic compositions and trace element abundances of volcaniclastic material deposited in both rear-arc and forearc settings are critical for inferring the compositional evolution of arc magmas in conditions where the arc basement is covered by thick sedimentary deposits. We target disaggregated volcaniclastic sandstones of Site U1438 (Unit III) to the west of the Kyushu-Palau Ridge and which record basaltic to andesitic magmatism from the early Izu-Bonin arc between 40 to 30 Ma. Unit III sandstones record a sharp increase in slab-derived components over time whilst Hf and Nd isotopic ratios remain little changed. Hafnium isotopic compositions of these sandstones overlap the more radiogenic boninites formed during the preceding phase of volcanism upon subduction initiation along the forearc and which trend towards Pacific-MORB isotopic compositions. However, the ε_{Hf} composition of these sandstones does not revert back to more radiogenic compositions consistent with an Indian-type MORB mantle and which is sampled in coeval tephra from the forearc (ODP Site 782) and in the preceding phase of magmatism upon subduction initiation (highly depleted basalts). This shift in isotopic ratios is at odds with trace element abundances and trace element ratios implying a contribution from oceanic sediments from a subducting slab. Addition of a Pacific MORB component as a melt or supercritical fluid allows resolution of this apparent paradox and coincides well with other localities where arc lavas with depleted MORB-like Nd–Hf characteristics are attributed to a MORB slab melt. A subducted Pacific MORB component is continuously identifiable in the products of Izu-Bonin volcanism beginning with the boninites in the nascent stage of arc growth and persists in the modern Izu-Bonin arc.

Declaration of Competing Interest

The authors declare that they have no known competing financial interests or personal relationships that could have appeared to influence the work reported in this paper.

ACKNOWLEDGMENTS

AM acknowledges support from the SNSF (grant 200020/135511 to Othmar Müntener and grant P2LAP2_171819 to AM) and Swiss IODP. IPS participation in IODP Exp.351

and postcruise research was funded from UK NERC grant (NE/M007782/1) This work was also supported by grants to GMY and MB from NSF (OCE-1537135), OCE-1624315 to MB, and IODP. RHV is grateful for support received from NSF OCE-1537861. The authors are grateful to J. Sexton (CEMS, University of South Carolina), A. Ulianov, O. Reubi (ISTE, University of Lausanne) and A. Vho (University of Bern) for their assistance with data collection. The work and assistance of the captain and crew of the D/V JOIDES Resolution and support from the International Ocean Discovery Program (IODP) are gratefully acknowledged. The authors are grateful for constructive reviews by M. Brounce, H. Freymouth and one anonymous reviewer that helped us to clarify and improve the paper. Editorial handling and additional comments by Associate Editor J. Day is gratefully acknowledged.

APPENDIX A. SUPPLEMENTARY MATERIAL

Supplementary data to this article can be found online at https://doi.org/10.1016/j.gca.2021.01.006.

REFERENCES

Arculus R. J. and Bloomfield A. L. (1992) Major-element chemistry of ashes from sites 782, 784, and 786 in the Bonin Forearc. In *Proceedings of the Ocean Drilling Program, Scientific Results, 125* (eds. P. Fryer, J. A. Pearce and L. B. Stokking). Ocean Drilling Program, College Station, TX, pp. 277–292.

Arculus R. J., Ishizuka O., Bogus K., Aljahdali M. H., Bandini-Maeder A. N., Barth A. P., Brandl P. A., do Monte Guerra R., Drab L., Gurnis M. C., Hamada M., Hickey-Vargas R. L., Jiang F., Kanayama K., Kender S., Kusano Y., Li H., Loudin L. C., Maffione M., Marsaglia K. M., McCarthy A., Meffre S., Morris A., Neuhaus M., Savov I. P., Sena Da Slva C. A., Tepley F. J., III, van der Land C., Yogodzinski G. M., and Zhang Z. (2015a). Site U1438. In Arculus R. J., Ishizuka O., Bogus K., and the Expedition 351 Scientists. Proceedings of the International Ocean Discovery Program, Expedition 351: Izu-Bonin-Mariana Arc Origins. College Station, TX (International Ocean Discovery Program).

Arculus R. J., Ishizuka O., Bogus K., Aljahdali M. H., Bandini-Maeder A. N., Barth A. P., Brandl P. A., do Monte Guerra R., Drab L., Gurnis M. C., Hamada M., Hickey-Vargas R. L., Jiang F., Kanayama K., Kender S., Kusano Y., Li H., Loudin L. C., Maffione M., Marsaglia K. M., McCarthy A., Meffre S., Morris A., Neuhaus M., Savov I. P., Sena Da Silva C. A., Tepley, III, F. J., van der Land C., Yogodzinski G. M. and Zhang Z. (2015b) A record of spontaneous subduction initiation in the Izu-Bonin-Mariana arc. *Nat. Geosci.* **8**(9), 728–733.

Arculus R. J., Gurnis M., Ishizuka O., Reagan M. K., Pearce J. A. and Sutherland R. (2019) How to create new subduction zones: a global perspective. *Oceanography* **32**(1), 160–174.

Barth A. P., Tani K., Meffre S., Wooden J. L., Coble M. A., Arculus R. J., Ishizuka O. and Shukle J. T. (2017) Generation of silicic melts in the early izu-bonin arc recorded by detrital zircons in proximal arc volcaniclastic rocks from the Philippine Sea. *Geochem., Geophys., Geosyst.* **18**(10), 3576–3591.

Bienvenu P., Bougault H., Joron J. L., Treuil M. and Dmitriev L. (1990) MORB alteration: rare-earth element/non-rare-earth hygromagmaphile element fractionation. *Chem. Geol.* **82**, 1–14.

Bloomer S. H. and Hawkins J. W. (1987) Petrology and geochemistry of boninitic series volcanic rocks from the Mariana trench. *Contrib. Mineral. Petrol.* **97**, 361–377.

Bouvier A., Vervoort J. D. and Patchett P. J. (2008) The Lu-Hf and Sm-Nd isotopic composition of CHUR: constraints from unequilibrated chondrites and implications for the bulk composition of terrestrial planets. *Earth Planet. Sci. Lett.* **273**, 48–57.

Brandl P. A., Hamada M., Arculus R. J., Johnson K., Marsaglia K. M., Savov I. P., Ishizuka O. and Li H. (2017) The arc arises: The links between volcanic output, arc evolution and melt composition. *Earth Planet. Sci. Lett.* **461**, 73–84.

Bryant C. J., Arculus R. J. and Eggins S. M. (2003) The geochemical evolution of the Izu-Bonin Arc System: a perspective from tephras recovered by deep-sea drilling. *Geochem., Geophys., Geosyst.* **4**(11), 1094.

Carter L. B., Skora S., Blundy J. D., De Hoog J. C. M. and Elliott T. (2015) An experimental study of trace element fluxes from subducted oceanic crust. *J. Petrol.* **56**(8), 1585–1606.

Chauvel C. and Blichert-Toft J. (2001) A hafnium isotope and trace element perspective on melting of the depleted mantle. *Earth and Planetary Science Letters* **190**(3–4), 137–151. https://doi.org/10.1016/S0012-821X(01)00379-X.

Chauvel C., Marini J. C., Plank T. and Ludden J. N. (2009) Hf–Nd input flux in the Izu-Mariana subduction zone and recycling of subducted material in the mantle. *Geochem., Geophys., Geosyst.* **10**(1).

Cosca M. A., Arculus R. J., Pearce J. A. and Mitchell J. G. (1998) Ar-40/Ar-39 and K-Ar geochronological age constraints for the inception and early evolution of the Izu-Bonin-Mariana Arc system. *Isl. Arc* **7**, 579–595.

DeCelles P. G., Ducea M. N., Kapp P. and Zandt G. (2009) Cyclicity in Cordilleran orogenic systems. *Nat. Geosci.* **2**(4), 251–257.

Egeberg P. K., Brunfelt A. O. and Stabel A. S. (1992) Characterization and correlation of megascopic tephras in site 792 cores fromthe Izu-Ogasawara forearc basin (Japan) by trace element and $^{87}Sr/^{86}Sr$ and $^{143}Nd/^{144}Nd$ isotopes. In *Proceedings of the Ocean Drilling Program, Scientific Results, 126* (eds. B. Taylor and K. Fujioka). Ocean Drilling Program, College Station, TX, pp. 457–465.

Freymuth H., Ivko B., Gill J. B., Tamura Y. and Elliott T. (2016) Thorium isotope evidence for melting of the mafic oceanic crust beneath the Izu arc. *Geochim. Cosmochim. Acta* **186**, 49–70.

Gale A., Dalton C. A., Langmuir C. H., Su Y. and Schilling J. G. (2013) The mean composition of ocean ridge basalts. *Geochem., Geophys., Geosyst.* **14**(3), 489–518.

Gill J. (1981) *Orogenic Andesites and Plate Tectonics*. Springer-Verlag, Berlin Heidelberg, p. 392.

Gill J. B., Hiscott R. N. and Vidal P. (1994) Turbidite geochemistry and evolution of the Izu-Bonin arc and continents. *Lithos* **33**(1–3), 135–168.

Govindaraju K. (1994) Compilation of working values and sample description for 383 geostandards. *Geostandards Newslett.* **18**, 1–158.

Hamada Morihis, Iwamori Hikar, Brandl Philipp A., Ushikubo Takayuk, Shimizu Kenj, Ito Moto, Li H and Savov Ivan P. (2020) Temporal evolution of proto-Izu–Bonin–Mariana arc volcanism over 10 Ma: constraints from statistical analysis of melt inclusion compositions. *J. Petrol.*.

Hanyu T., Tatsumi Y., Nakai S. I., Chang Q., Miyazaki T., Sato K., Tani K., Shibata T. and Yoshida T. (2006) Contribution of slab melting and slab dehydration to magmatism in the NE Japan arc for the last 25 Myr: Constraints from geochemistry. *Geochem., Geophys., Geosyst.* **7**(8).

Hein J. R. and Scholl D. W. (1978) Diagenesis and distribution of late Cenozoic volcanic sediment in the southern Bering Sea. *Geol. Soc. Am. Bull.* **89**(2), 197–210.

Hermann J. and Rubatto D. (2009) Accessory phase control on the trace element signature of sediment melts in subduction zones. *Chemical Geology* **265**(3–4), 512–526. https://doi.org/10.1016/j.chemgeo.2009.05.018.

Heyworth Z., Knesel K. M., Turner S. P. and Arculus R. J. (2011) Pb-isotopic evidence for rapid trench-parallel mantle flow beneath Vanuatu. *J. Geol. Soc.* **168**(1), 265–271.

Hickey-Vargas R., Yogodzinski G. M., Ishizuka O., McCarthy A., Bizimis M., Kusano Y., Savov I. P. and Arculus R. (2018) Origin of depleted basalts during subduction initiation and early development of the Izu-Bonin-Mariana island arc: evidence from IODP expedition 351 site U1438, Amami-Sankaku basin. *Geochim. Cosmochim. Acta* **229**, 85–111.

Hochstaedter A., Gill J., Peters R., Broughton P., Holden P. and Taylor B. (2001) Across-arc geochemical trends in the Izu-Bonin arc: contributions from the subducting slab. *Geochem., Geophys., Geosyst.* **2**(7).

Ishizuka O., Kimura J. I., Li Y. B., Stern R. J., Reagan M. K., Taylor R. N., Ohara Y., Bloomer S. H., Ishii T., Hargrove, III, U. S. and Haraguchi S. (2006) Early stages in the evolution of Izu-Bonin arc volcanism: New age, chemical, and isotopic constraints. *Earth Planet. Sci. Lett.* **250**(1–2), 385–401.

Ishizuka O., Tani K., Reagan M. K., Kanayama K., Umino S., Harigane Y., Sakamoto I., Miyajima Y., Yuasa M. and Dunkley D. J. (2011a) The timescales of subduction initiation and subsequent evolution of an oceanic island arc. *Earth Planet. Sci. Lett.* **306**, 229–240.

Ishizuka O., Taylor R. N., Yuasa M. and Ohara Y. (2011b) Making and breaking an island arc: a new perspective from the Oligocene Kyushu-Palau arc, Philippine Sea. *Geochem., Geophys., Geosyst.* **12**(5).

Ishizuka O., Hickey-Vargas R., Arculus R. J., Yogodzinski G. M., Savov I. P., Kusano Y., McCarthy A., Brandl P. A. and Sudo M. (2018) Age of Izu–Bonin–Mariana arc basement. *Earth Planet. Sci. Lett.* **481**, 80–90.

Ishizuka O., Taylor R. N., Umino S. and Kanayama K. (2020) Geochemical evolution of arc and slab following subduction initiation: a record from the Bonin Islands, Japan. *J. Petrol.*.

Jackson S. E. (2008). LAMTRACE data reduction software for LA-ICP-MS. In Laser Ablation ICP-MS in the Earth Sciences: Current Practices and Outstanding Issues (ed. P. Sylvester). Mineralogical Association of Canada, Short Course Series, 40, pp. 305–307.

Jochum K. P., Weis U., Stoll B., Kuzmin D., Yang Q., Raczek I., Jacob D. E., Stracke A., Birbaum K., Frick D. A. and Günther D. (2011) Determination of reference values for NIST SRM 610–617 glasses following ISO guidelines. *Geostand. Geoanal. Res.* **35**(4), 397–429.

Johnson K., Waldman, R. and Marsaglia K. M. (2017). Data report: sedimentary columns with facies and bedding for Units II-IV at IODP Site U1438. In Proceedings of the International Ocean Discovery Program, Volume 351. Izu–Bonin–Mariana Arc Origins (eds. R. J. Arculus, O. Ishizuka, K. Bogus and Expedition 351 Scientists). International Ocean Discovery Program, College Station, TX.

Kay R. W. (1978) Aleutian magnesian andesites: melts from subducted Pacific Ocean crust. *J. Volcanol. Geotherm. Res.* **4**, 117–132.

Kay S. M., Godoy E. and Kurtz A. (2005) Episodic arc migration, crustal thickening, subduction erosion, and magmatism in the south-central Andes. *Geol. Soc. Am. Bull.* **117**(1–2), 67–88.

Kelemen P. B. (1995) Genesis of high Mg# andesites and the continental crust. *Contrib. Miner. Petrol.* **120**, 1–19.

Kelemen P. B., Yogodzinski G. M. and Scholl D. W. (2003). Along-strike variation in the Aleutian island arc: genesis of high Mg# andesite and implications for continental crust. In Inside the Subduction Factory, Geophysical Monograph Series 138 (ed. J. Eiler), AGU, Washington, D.C., pp. 223–276.

Kessel R., Schmidt M. W., Ulmer P. and Pettke T. (2005) Trace element signature of subduction-zone fluids, melts and supercritical liquids at 120–180 km depth. *Nature* **437**(7059), 724–727.

Kimura J. I., Nagahashi Y., Satoguchi Y. and Chang Q. (2015) Origins of felsic magmas in Japanese subduction zone: Geochemical characterizations of tephra from caldera-forming eruptions< 5 Ma. *Geochem. Geophys. Geosyst.* **16**(7), 2147–2174.

Lallemand S. (2016) Philippine Sea Plate inception, evolution, and consumption with special emphasis on the early stages of Izu-Bonin-Mariana subduction. *Prog. Earth Planet. Sci.* **3**, 15.

Li H. Y., Taylor R. N., Prytulak J., Kirchenbaur M., Shervais J. W., Ryan J. G., Godard M., Reagan M. K. and Pearce J. A. (2019) Radiogenic isotopes document the start of subduction in the Western Pacific. *Earth Planet. Sci. Lett.* **518**, 197–210.

Li Y.-B., Kimura J.-I., Machida S., Ishii T., Ishiwatari A., Maruyama S., Qiu H.-N., Ishikawa T., Kato Y., Haraguchi S., Takahata N., Hirahara Y. and Miyazaki T. (2013) High-Mg adakite and low-Ca boninite from a Bonin fore-arc seamount: Implications for the reaction between slab melts and depleted mantle. *J. Petrol.* **54**, 1149–1175.

Liang M., Guo Z., Kahmann A. J. and Oldfield F. (2009) Geochemical characteristics of the Miocene eolian deposits in China: their provenance and climate implications. *Geochem., Geophys., Geosyst.* **10**(4).

Louvel M., Sanchez-Valle C., Malfait W. J., Testemale D. and Hazemann J. L. (2013) Zr complexation in high pressure fluids and silicate melts and implications for the mobilization of HFSE in subduction zones. *Geochim. Cosmochim. Acta* **104**, 281–299.

McCarthy A., Yogodzinski G., Tepley, III, F. J., Bizimis M., Arculus R. and Ishizuka O. (2019) Isotopic characteristics of Neogene-Quaternary tephra from IODP Site U1438: a record of explosive volcanic activity in the Kyushu-Ryukyu arc. *Geochem. Geophys. Geosyst.* **20**, 2318–2333.

McDonough W. F. and Sun S. S. (1995) The composition of the Earth. *Chem. Geol.* **120**(3–4), 223–253.

Miyashiro A. (1974) Volcanic rock series in island arcs and active continental margins. *Am. J. Sci.* **274**(4), 321–355.

Monzier M., Danyushevsky L. V., Crawford A. J., Bellon H. and Cotton J. (1993) High-Mg andesites from the southern termination of the New Hebrides island arc (SW Pacific). *J. Volcanol. Geoth. Res.* **57**, 193–217.

Münker C., Weyer S., Scherer E. and Mezger K. (2001) Separation of high field strength elements (Nb, Ta, Zr, Hf) and Lu from rock samples for MC-ICPMS measurements. *Geochem., Geophys., Geosyst.* **2**(12).

Natland J. H. and Tarney J. (1981). Petrologic evolution of the Mariana arc and back-arc system—A synthesis of drilling results in the south Philippine Sea. In Initial reports DSDP, vol. 60 (eds. D. M. Hussong, S. Uyeda, et al.). U.S. Government Printing Office, Washington, D.C., pp. 877–908.

Patino L. C., Velbel M. A., Price J. R. and Wade J. A. (2003) Trace element mobility during spheroidal weathering of basalts and andesites in Hawaii and Guatemala. *Chem. Geol.* **202**(3–4), 343–364.

Patriat M., Falloon T., Danyushevsky L., Collot J., Jean M. M., Hoernle K., Hauff F., Maas R., Woodhead J. D. and Feig S. T. (2019) Subduction initiation terranes exposed at the front of a 2 Ma volcanically-active subduction zone. *Earth Planet. Sci. Lett.* **508**, 30–40.

Pearce J. A. (1982) Trace element characteristics of lavas from destructive plate boundaries. In *Orogenic Andesites and Related*

Rocks (ed. R. S. Thorpe). John Wiley and Sons, Chichester, England, pp. 528–548.

Pearce J. A., van der Laan S. R., Arculus R. J., Murton B. J., Ishii T., Peate D. W. and Parkinson I. (1992) Boninite and harzburgite from Leg 125 (Bonin-Mariana Forearc): a case study of magma genesis during the initial stages of subduction. *Proc. ODP Sci. Results* **125**, 623–659.

Pearce J. A., Baker P. E., Harvey K. P. and Luft I. W. (1995) Geochemical evidence for subduction fluxes, mantle melting and fractional crystallization beneath the South Sandwich island arc. *J. Petrol.* **36**, 1073–1109.

Pearce J. A., Kempton P. D., Nowell G. M. and Noble S. R. (1999) Hf-Nd element and isotope perspective on the nature and provenance of mantle and subduction components in Western Pacific arc-basin systems. *J. Petrol.* **40**(11), 1579–1611.

Pearce J. A., Stern R. J., Bloomer S. H. and Fryer P. (2005) Geochemical mapping of the Mariana arc-basin system: Implications for the nature and distribution of subduction components. *Geochem., Geophys., Geosyst.* **6**(7).

Pearce J. A., Kempton P. D. and Gill J. B. (2007) Hf–Nd evidence for the origin and distribution of mantle domains in the SW Pacific. *Earth Planet. Sci. Lett.* **260**(1–2), 98–114.

Pin C. and Zalduegui J. F. S. (1997) Sequential separation of light rare-earth elements, thorium and uranium by miniaturized extraction chromatography: application to isotopic analyses of silicate rocks. *Anal. Chim. Acta* **339**, 79–89.

Pineda-Velasco I., Kitagawa H., Nguyen T. T. and Nakamura E. (2018) Production of high-Sr andesite and dacite magmas by melting of subducting oceanic lithosphere at propogating slab tears. *J. Geophys. Res. Solid Earth* **123**(5), 3698–3728.

Plank T. (2005) Constraints from thorium/lanthanum on sediment recycling at subduction zones and the evolution of continents. *J. Petrol.* **46**, 921–944.

Plank T., Kelley K. A., Murray R. W. and Stern L. Q. (2007) Chemical composition of sediments subducting at the Izu-Bonin trench. *Geochem., Geophys., Geosyst.* **8**(4), Q04I16.

Rapp R. P., Shimizu N., Norman M. D. and Applegate G. S. (1999) Reaction between slab-derived melts and peridotite in the mantle wedge: experimental constraints at 3.8 GPa. *Chem. Geol.* **160**(4), 335–356.

Reagan M. K., Ishizuka O., Stern R. J., Kelley K. A., Ohara Y., Blichert-Toft J., Bloomer S. H., Cash J., Fryer P., Hanan B. B., Hickey-Vargas R., Ishii T., Kimura J.-I., Peate D. W., Rowe M. C. and Woods M. (2010) Fore–arc basalts and subduction initiation in the Izu–Bonin–Mariana system. *Geochem. Geophys. Geosyst.* **11**(3).

Reagan M. K., Heaton D. E., Schmitz M. D., Pearce J. A., Shervais J. W. and Koppers A. A. (2019) Forearc ages reveal extensive short-lived and rapid seafloor spreading following subduction initiation. *Earth Planet. Sci. Lett.* **506**, 520–529.

Robertson A. H., Kutterolf S., Avery A., Baxter A. T., Petronotis K., Acton G. D., Carvallo C. and Schindlbeck J. C. (2018) Depositional setting, provenance, and tectonic-volcanic setting of Eocene-Recent deep-sea sediments of the oceanic Izu-Bonin forearc, northwest Pacific (IODP Expedition 352). *Int. Geol. Rev.* **60**(15), 1816–1854.

Savov I. P., Hickey-Vargas R., Dantonio M. A., Ryan J. G. and Spadea P. (2006) Petrology and geochemistry of West Philippine Basin basalts and early Palau-Kyushu arc volcanic clasts from ODP Leg 195, Site 1201D: implications for the early history of the Izu–Bonin–Mariana arc. *J. Petrol.* **47**(2), 277–299.

Schindlbeck J. C., Kutterolf S., Straub S. M., Andrews G. D., Wang K. L. and Mleneck-Vautravers M. J. (2018) One Million Years tephra record at IODP Sites U1436 and U1437: insights into explosive volcanism from the Japan and Izu arcs. *Isl. Arc* **27**(3). https://doi.org/10.1111/iar.12244 e12244.

Shervais J. W., Reagan M., Haugen E., Almeev R. R., Pearce J. A., Prytulak J., Ryan J. G., Whattam S. A., Godard M., Chapman T. and Li H. (2019) Magmatic response to subduction initiation: Part 1. Fore-arc basalts of the Izu-Bonin arc from IODP Expedition 352. *Geochem., Geophys., Geosyst.* **20**(1), 314–338.

Shipboard Scientific Party (1990). Site 782. In Proc. ODP, Initial Reports, 125 (eds. P. Fryer, J. A. Pearce, L. B. Stokking, et al.). Ocean Drilling Program, College Station, TX, pp. 197–252.

Skora S. and Blundy J. (2010) High-pressure hydrous phase relations of radiolarian clay and implications for the involvement of subducted sediment in arc magmatism. *J. Petrology* **51** (11), 2211–2243. https://doi.org/10.1093/petrology/egq054.

Straub S. (2003) The evolution of the Izu Bonin-Mariana volcanic arcs (NW Pacific) in terms of major element chemistry. *Geochem. Geophys. Geosyst.* **4**(2), 1018.

Straub S. M., Layne G. D., Schmidt A. and Langmuir C. H. (2004) Volcanic glasses at the Izu arc volcanic front: New perspectives on fluid and sediment melt recycling in subduction zones. *Geochem. Geophys. Geosyst.* **5**, Q01007.

Straub S. M., Goldstein S. L., Class C., Schmidt A. and Gomez-Tuena A. (2010) Slab and mantle controls on the Sr–Nd–Pb–Hf isotope evolution of the post 42 Ma Izu-Bonin volcanic arc. *J. Petrol.* **51**(5), 993–1026.

Straub S. M., Woodhead J. D. and Arculus R. J. (2015) Temporal evolution of the Mariana Arc: mantle wedge and subducted slab controls revealed with a tephra perspective. *J. Petrol.* **56**(2), 409–439.

Straub M. S. (2017). Compilation of published major and trace elements and Sr-Nd-Pb-Hf isotope ratios of Quaternary-age arc volcanic rocks from 9 arc settings Interdisciplinary Earth Data Alliance (IEDA).

Shirey S. B. and Hanson G. N. (1984) Mantle-derived Archaean monozodiorites and trachyandesites. *Nature* **310**, 222–224.

Stern R. J. and Bloomer S. H. (1992) Subduction zone infancy; examples from the Eocene Izu-Bonin-Mariana and Jurassic California arcs. *Geol. Soc. Am. Bull.* **104**, 1621–1636.

Taylor S. R. and White A. J. R. (1965) Geochemistry of andesites and the growth of continents. *Nature* **208**, 271–273.

Tollstrup D. L. and Gill J. B. (2005) Hafnium systematics of the Mariana arc: evidence for sediment melt and residual phases. *Geology* **33**(9), 737–740.

Tollstrup D., Gill J., Kent A., Prinkey D., Williams R., Tamura Y. and Ishizuka O. (2010) Across-arc geochemical trends in the Izu-Bonin arc: contributions from the subducting slab, revisited. *Geochem. Geophys. Geosyst.* **11**(1).

Tsay A., Zajacz Z., Ulmer P. and Sanchez-Valle C. (2017) Mobility of major and trace elements in the eclogite-fluid system and element fluxes upon slab dehydration. *Geochim. Cosmochim. Acta* **198**, 70–91.

von Huene R. and Scholl D. W. (1991) Observations at convergent margins concerning sediment subduction, subduction erosion, and the growth of continental crust. *Rev. Geophys.* **29**, 279–316.

Yogodzinski G. M., Volynets O. N., Koloskov A. V., Seliverstov N. I. and Matvenkov V. V. (1994) Magnesian andesites and the subduction component in a strongly calc-alkaline series at Piip Volcano, far western Aleutians. *J. Petrol.* **35**(1), 163–204.

Yogodzinski G. M., Kay R. W., Volynets O. N., Koloskov A. V. and Kay S. M. (1995) Magnesian andesite in the western Aleutian Komandorsky region: Implications for slab melting and processes in the mantle wedge. *Geol. Soc. Am. Bull.* **107**, 505–519.

Yogodzinski G. M., Lees J. M., Churikova T. G., Dorendorf F., Wörner G. and Volynets O. N. (2001) Geochemical evidence for the melting of subducting oceanic lithosphere at plate edges. *Nature* **409**, 500–504.

Yogodzinski G. M., Brown S. T., Kelemen P. B., Vervoort J. D., Portnyagin M., Sims K. W., Hoernle K., Jicha B. R. and Werner R. (2015) The role of subducted basalt in the source of island arc magmas: evidence from seafloor lavas of the western Aleutians. *J. Petrol.* **56**(3), 441–492.

Yogodzinski G. M., Kelemen P. B., Hoernle K., Brown S. T., Bindeman I., Vervoort J. D., Sims K. W., Portnyagin M. and Werner R. (2018) Sr and O isotopes in western Aleutian seafloor lavas: Implications for the source of fluids and trace element character of arc volcanic rocks. *Earth Planet. Sci. Lett.* **475**, 169–180.

Yogodzinski G. M., Bizimis M., Hickey-Vargas R., McCarthy A., Hocking B. D., Savov I. P., Ishizuka O. and Arculus R. (2018) Implications of Eocene-age Philippine Sea and forearc basalts for initiation and early history of the Izu-Bonin-Mariana arc. *Geochim. Cosmochim. Acta* **228**, 136–156.

Yogodzinski G. M., Vervoort J. D., Brown S. T. and Gerseny M. (2010) Subduction controls of Hf and Nd isotopes in lavas of the Aleutian island arc. *Earth Planet. Sci. Lett.* **300**, 226–238. https://doi.org/10.1016/j.epsl.2010.09.035.

Vallier T. L., Windom K. E., Seifert K. E. and Thiede J. (1980) Volcanic rocks cored on Hess Rise, western Pacific ocean. *Nature* **286**(5768), 48–50.

Vervoort J. D., Plank T. and Prytulak J. (2011) The Hf–Nd isotopic composition of marine sediments. *Geochim. Cosmochim. Acta* **75**(20), 5903–5926.

Waldman R. J., Marsaglia K. M., Hickey-Vargas R., Ishizuka O., Johnson K. E., McCarthy A., Yogodzinski G., Samajpati E., Laxton K., Savov I. P., Meffre S., Arculus R. J., Bandini A. N., Barth A., Bogud K., Brandl P. A., Gurnis M. and Jiang F. (2020) Sedimentary and volcanic record of the nascent IBM arc from IODP Site U1438. *Geol. Soc. Am. Bull.*.

Weis D., Maerschalk C., Barling J., Williams G. A., Hanano D., Pretorius W., Mattielli N., Scoates J. S., Goolaerts A., Friedman R. M. and Mahoney J. B. (2006) High-precision isotopic characterization of USGS reference materials by TIMS and MC-ICP-MS. *Geochem. Geophys. Geosys.* **7**.

Weis D., Kieffer B., Hanano D., Silva I. N., Barling J. and Pretorius W. (2007) Hf isotope compositions of U.S. Geological Survey reference materials. *Geochem. Geophys. Geosys.* **8**.

Workman R. K. and Hart S. R. (2005) Major and trace element composition of the depleted MORB mantle (DMM). *Earth Planet. Sci. Lett.* **231**(1–2), 53–72.

Associate editor: James M.D. Day